# 1 The influence of a rock glacier on the riverbed hydrological system

- 2 Bastien Charonnat<sup>1,6,7</sup>, Michel Baraer<sup>1,6,7</sup>, Eole Valence<sup>2,6</sup>, Janie Masse-Dufresne<sup>1,6,7</sup>, Chloé Monty<sup>3</sup>,
- 3 Kaiyuan Wang<sup>4</sup>, Elise Devoie<sup>5</sup>, Jeffrey M. McKenzie<sup>2</sup>

4

7

- 5 <sup>1</sup>Hydrology, Climate and Climate Change laboratory École de technologie supérieure (ÉTS), Montreal, Quebec, Canada
- 6 <sup>2</sup>Department of Earth and Planetary Science McGill University, Montreal, Quebec, Canada
  - <sup>3</sup> Department of Earth Sciences Simon Fraser University, Burnaby, British Columbia, Canada
- 8 <sup>4</sup>Department of Earth, Environmental & Planetary Sciences Brown University, Providence, Rhode Island, United States
- 9 <sup>5</sup> Civil Engineering department Queen's University, Kingston, Ontario, Canada
- 10 <sup>6</sup> GEOTOP (Research Centre on the Dynamics of the Earth System), Montreal, Quebec, Canada
  - <sup>7</sup> CentrEau (Ouebec Research Water Centre), Ouebec City, Ouebec, Canada

11 12 13

14

Correspondence to: Bastien Charonnat (bastien.charonnat.1@ens.etsmtl.ca)

## Abstract

- 15 Climate change is accelerating cryosphere degradation in mountain regions, and altering hydrological and geomorphological
- dynamics within deglaciating catchments. Rock glaciers, which degrade slower than glaciers, can exert a prolonged influence
- 17 on water resources in alpine watersheds. This study investigates both the direct and indirect influences of a rock glacier on the
- 18 Shár Shaw Tagà (Grizzly Creek) riverbed in the St. Elias Mountains (Yukon, Canada). We applied a unique multimethod
- 19 approach combining hydro-physicochemical and isotopic characterization, drone-based thermal infrared (TIR) imagery, and
- visible time-lapse (TL) imagery.
- 21 Results reveal that the rock glacier's geomorphic and thermal properties constrain the riverbed and its underlying alluvial
- 22 aquifer, driving shallow groundwater resurgence. These indirect disruptions promote downstream cryo-hydrological processes
- by facilitating aufeis formation and modifying the physicochemical properties of surface water. In contrast, direct hydrological
- 24 influence from the rock glacier's internal drainage system to downstream surface waters appears minimal. This configuration
- is transitional, as the constraint imposed by ground ice is expected to diminish with progressive permafrost degradation.
- 26 Overall, this study identifies the critical yet transient role of rock glaciers in alpine hydrology. Beyond their internal
- 27 hydrological behaviour, they shape catchment hydrology through geomorphic controls. Our findings highlight the need to
- account for indirect effects when evaluating hydrological dynamics in deglaciating catchments.

# 1. Introduction

29

- 30 Climate change is profoundly transforming mountain regions, where the cryosphere has a critical role in regulating water
- 31 resources that sustain downstream ecosystems and communities. With rising global temperatures, high mountain areas are

- 32 experiencing accelerated deglaciation, characterized by glacial retreat and permafrost thaw (Hock et al., 2019). These processes
- drive rapid geomorphological and hydrological reconfigurations in proglacial systems (Carrivick and Heckmann, 2017).
- 34 Understanding how cryosphere degradation affects mountain hydrology and hydrogeology is therefore essential for predicting
- future water availability (Hayashi, 20220; van Tiel et al., 2024).
- 36 Among cryospheric features, rock glaciers degrade the slowest, continuing to influence hydrology long after glaciers have
- 37 retreated (Bolch and Marchenko, 2009; Harrison et al., 2021; Jones et al., 2021). Rock glaciers are tongue-shaped landforms
- 38 composed of rocky debris and ice, which creep due to the deformation of the ice-debris matrix, concentrated in the shear
- 39 horizon (Arenson et al., 2002). They are commonly found in high mountain environments and occur in both discontinuous and
- 40 continuous permafrost zones (Barsch, 1996).
- 41 Historically, research on rock glaciers has focused primarily on two aspects: their hydrological behaviour, particularly their
- 42 direct influence on catchment hydrology, and their geomorphological dynamics. In this study, we differentiate between direct
- 43 hydrological influence (i.e., related to rock glacier internal hydrological processes and resulting outflows) and indirect
- 44 hydrological influence (i.e., arising from external processes linked to rock glacier dynamics, such as geomorphic obstruction
- of a riverbed, limiting hydraulic conductivity and potentially altering surface and shallow groundwater flow patterns).
- 46 Direct hydrological influence of rock glaciers involves buffering catchment surface water discharge, by sustaining baseflow
- 47 and attenuating discharge response to intense precipitation peaks (Bearzot et al., 2023; Reato et al., 2022; Wagner et al., 2021).
- 48 A rock glacier's hydrological behaviour is closely tied to its internal distribution of frozen and liquid water (Harrington et al.,
- 49 2018; Wagner et al., 2016; Winkler et al., 2016). Unfrozen layers in summer can act as reservoirs and conduits for water flow
- 50 (Halla et al., 2021; Harrington et al., 2018; Navarro et al., 2023; Wagner et al., 2020). In addition to liquid water, intact rock
- 51 glaciers (i.e., containing frozen content) store significant volumes of solid water as interstitial or massive ice (Chakravarthi et
- al., 2022; Halla et al., 2021; Jones et al., 2018; Wagner et al., 2021). However, internal ice melt typically contributes only
- 53 minimally to total rock glacier discharge (Arenson et al., 2022). Rock glaciers also directly influence downstream water quality
- by increasing solute concentrations (Colombo et al., 2018; Colombo et al., 2019; Schreder et al., 2023; Engel et al., 2019;
- Wanner et al., 2023; Zarroca et al., 2021) and cooling stream temperatures (Bearzot et al., 2023; Brighenti et al., 2019;
- 56 Colombo et al., 2020).
- 57 In addition, rock glaciers can exert indirect hydrological effects, as they are dynamic landforms that may advance, constrain,
- 58 or even dam riverbeds. Such effects have been reported in High Asia (Blöthe et al., 2019; Falatkova et al., 2020; Hewitt, 2014)
- 59 and the Alps (Colombo et al., 2020). Furthermore, topographic changes driven by glacial retreat and paraglacial processes can
- 60 force channel confinement (Marren and Toomath, 2014). Climate change has intensified rock glacier movement (Delaloye et
- al., 2010; Kummert et al., 2019; PERMOS, 2019), sometimes causing destabilization (Marcer et al., 2021) and channel
- disruption (Sorg et al., 2015). Additionally, sudden mass movements, such as the catastrophic collapse of rock glacier lobes,
- have triggered debris flows with downstream geomorphic impacts (Bodin et al., 2015; Scotti et al., 2017). Riverbeds and
- outwash plains play an important role in sustaining baseflow and aquatic habitats (Käser and Hunkeler, 2016; Müller et al.,

- 65 2024). However, to our knowledge, the indirect hydrological effects of rock glacier dynamics have not yet been assessed or compared with the direct effects of rock glaciers.
- The objective of this study is to address this research gap by simultaneously examining the direct and indirect hydrological influences of a rock glacier extending into a valley floor. Specifically, we aim to elucidate the underlying processes and anticipate the potential evolution of the system. We focus on surface water and shallow groundwater fluxes within a section of the Shár Shaw Tagà River in the St. Elias Mountains, Yukon, Canada, where the riverbed is constrained by the rock glacier.
- To reach this objective, we use a multimethod approach that combines observational techniques and naturel tracer analyses in two steps:
  - Monitoring and surveying of groundwater exfiltration, hypothesized to occur within the constrained river section, and
    causing significant outflows and winter aufeis formation. To assess the presence of important groundwater outflows
    in this section, we use drone-based thermal infrared (TIR) surveys, time-lapse monitoring and radon activities
    measurements.
  - 2. Physico-hydrochemical characterization to distinguish outflows associated with either the direct or the indirect influences of the rock glacier. We use synoptic sampling and hydrochemical analyses to characterize distinct water sources and their relative contributions.
  - The novelty of this research lies in its simultaneous assessment of direct and indirect hydrological influences of a rock glacier on catchment hydrology. Our findings highlight the complex and dynamic role of rock glaciers in alpine catchment systems and provide insights applicable to similar environments worldwide.

# 2. Study site

73

74

75

76

77

78 79

80

81

82

83

- 84 Shár Shaw Tagà, meaning Grizzly Creek in the Southern Tutchone indigenous language, is a 32 km² glacierized catchment
- 85 located within the traditional lands of the Kluane First Nation and the White River First Nation (Fig. 1a). It is within the Kluane
- National Park and Reserve in the St. Elias Mountains, southwestern Yukon Territory, Canada (61°05'13" N, 139°07'18" W).
- 87 The eastern flank of the St. Elias Mountains experiences a dry subarctic climate, characterized by annual precipitation ranging
- from 300 mm yr<sup>-1</sup> to 500 mm yr<sup>-1</sup> and a mean annual temperature between -8 °C and -12 °C (Wahl et al., 1987).
- 89 Publications prior to 2024 referred to the area by the toponym "Grizzly Creek" rather than Shár Shaw Tagà. The upper Shár
- 90 Shaw Tagà catchment (Fig. 1b) contains eight glaciers, the largest of which is G-A1, covering an area of 3.2 km<sup>2</sup>. Due to its
- 91 heavily fractured bedrock lithology and steep slopes, the valley is characterized by significant mass wasting processes and
- 92 depositional features, including nine previously identified rock glaciers (Johnson, 1978; Evin et al., 1997). Of these nine rock
- 93 glaciers, seven extend into the riverbed along the valley floor, with some exerting considerable geomorphological constraints
- 94 on the stream.

95

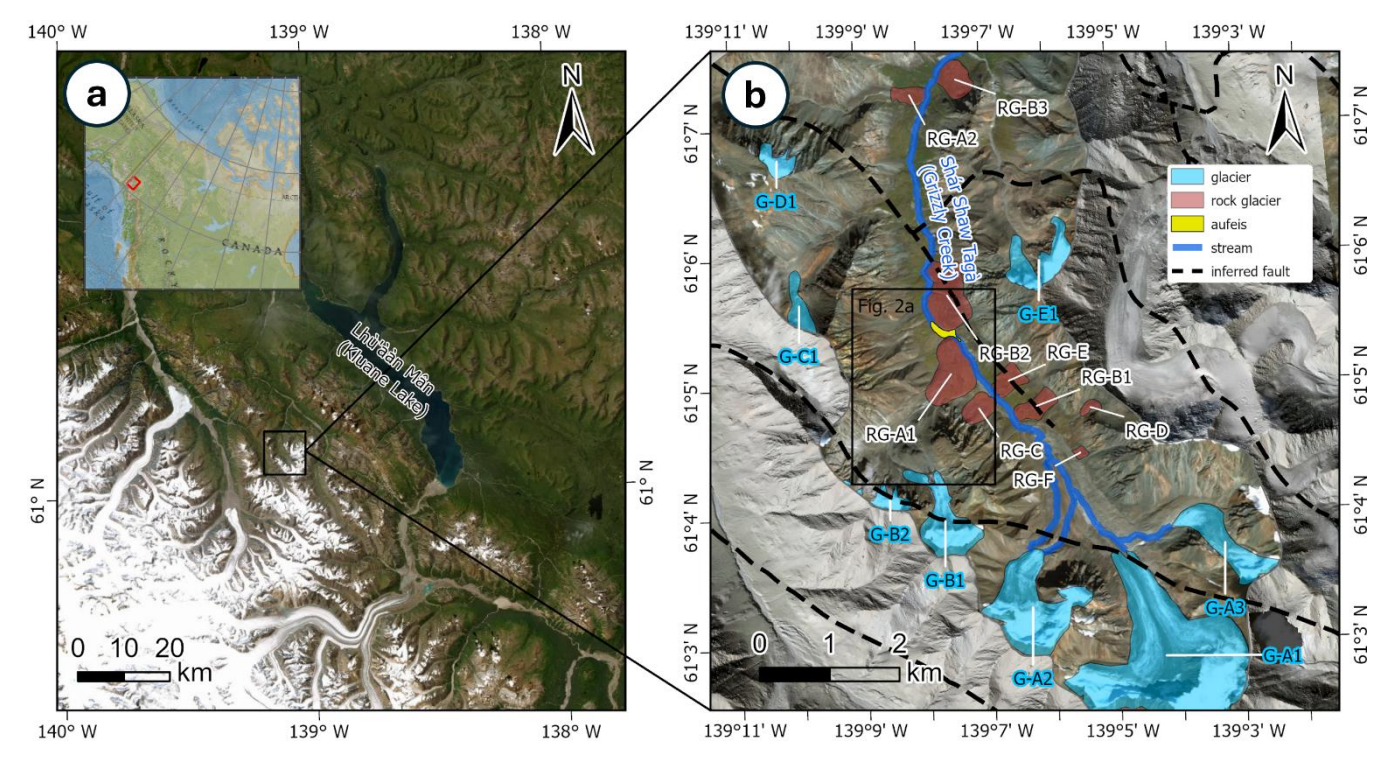


Fig. 1: (a) Overview map showing the location of the Shár Shaw Tagà valley in southwestern Yukon, Canada. (b) Enlarged view of the study area from panel (a), highlighting key geomorphological features. The black frame outlines the extent of the map shown in Fig. 2a. ArcticDEM data: Polar Geospatial Center (Porter et al., 2023). Basemap credits: Esri.

The present study focuses on the RG-A1 rock glacier, located on the western side of the upper Shár Shaw Tagà valley. The front of RG-A1 advances in the valley, constraining the Shár Shaw Tagà River against the opposing talus slope. RG-A1 spans elevations between 1700 and 1850 m a.s.l. The southern lobes of RG-A1 appear older, characterized by vegetation cover and a smoother frontal morphology, while the northern lobes are younger, with sparse or absent vegetation, sharper forms, and a steeper front (Johnson, 1978). Based on geophysical surveys, Evin et al. (1997) report a 20 to 40 m thick frozen layer as well as the presence of massive ice lenses at depth in RG-A1.

The outwash plains upstream and downstream of RG-A1 are separated by a "narrow section" of the Shár Shaw Tagà River, which can be divided into two subsections: N1 and N2 (Fig. 2). N1 extends from the outlet of the upstream outwash plain to a bedrock outcrop visible on the opposite talus slope to RG-A1. N2 extends from this bedrock outcrop to the outlet of the "narrow section", where the river reaches the downstream outwash plain. Although previous studies did not classify the talus slope opposed to RG-A1 as a rock glacier, it is suspected to be a protalus rampart (or small active rock glacier) based on environmental and topographic criteria outlined in Scapozza (2015). We noted the absence of an upstream permanent snow field, the presence of coarse boulders in the upslope area, a steep front with exposed fine sediments, and a juxtaposition and superimposition to other rock glaciers.

In 1974, Johnson (1978) observed that meltwater drained into a sinkhole located in the rooting zone of RG-A1 (at approximately 1850 m a.s.l.), with no major resurgence observed at its front (at 1700 m a.s.l.). In 1975, a new sinkhole was observed upstream of the first one, and a significant resurgence was reported on the northern part of RG-A1. Dry channels on the surface of RG-A1 in 1975 were interpreted by Johnson as abandoned surface drainage pathways, highlighting the dynamic and variable hydrological behaviour of RG-A1. Field observations by our team from 2018 to 2023 indicate no significant visible outlet from the rock glacier, despite its position downstream of an 8 km² subcatchment containing the G-B1 and G-B2 glaciers. The only visible outlets consist of low-discharge springs around the RG-A1 front, particularly concentrated along the N1 subsection. The lack of surface outflow from the rock glacier suggests subsurface connectivity with the Shár Shaw Tagà

123 River.

115

116

117

118

119

120

121

122

126

127

128

131

132

134

135

144

145

During low-discharge periods, such as in June 2023, we observed infiltration of Shár Shaw Tagà River water into the riverbed,

leaving the channel dry before the outwash plain upstream of RG-A1. Flow re-emerged in the N1 subsection, close to the rock

glacier's front, visually sustained by springs and seepage. Additional subsurface flow paths are evident in winter through aufeis

formation in the downstream outwash plain, documented by field observations since 2018 and on satellite imagery, while no

aufeis has been detected upstream between 2018 and 2023. Aufeis (or icings) are layered ice accumulations that develop when

groundwater outflows persist under sub-zero temperatures (Ensom et al., 2020).

130 The configuration of RG-A1, which constrains the riverbed, together with these groundwater observations in the "narrow

section," supports our hypothesis that the rock glacier exerts both direct and indirect hydrological influence on the riverbed

system. Accordingly, our methodology focuses on characterizing the sources and impacts of groundwater exfiltration in this

133 section.

#### 3. Methods

#### 3.1 Monitoring and surveying of groundwater exfiltration

# **3.1.2 TIR survey**

Aerial and handheld thermal infrared (TIR) devices have been demonstrated as effective tools for mapping groundwater discharge into streams (Toran, 2019). Specifically, drone-based TIR technology allows for high spatial resolution observations of surface water–groundwater interactions (Vélez-Nicolás et al., 2021). Two common approaches for TIR surveys were considered: 1) generating stream temperature maps using high-definition TIR image orthomosaics from overlapping images (e.g., Abolt et al., 2018; Casas-Mulet et al., 2020; Rautio et al., 2015), and 2) using TIR videos or real-time scans (handheld or drone-based) to visualize mixing plumes and record GPS coordinates of observed points (e.g., Barclay et al., 2022; Briggs

143 et al., 2016; Iwasaki et al., 2023).

Georeferenced thermal maps provide mesoscale coverage but require stable flying conditions, ground control points, and

extensive post-processing (Webb et al., 2008). In contrast, TIR video or live scans enable real-time visualization of mixing

dynamics at smaller scales (Antonelli et al., 2017). To identify and characterize cold groundwater emergence zones, we adopted the TIR video approach, which relies on relative temperature contrasts between stream water and suspected groundwater inflows rather than precise absolute temperatures. Previous studies have demonstrated that TIR video effectively highlights such contrasts even without embedded temperature scales (Antonelli et al., 2017; Briggs et al., 2016; Iwasaki et al., 2023, 2024). Drone-based TIR video surveys were conducted on 28 June 2024, between 08:00 and 10:00, to maximize the coverage of shaded sections of the stream. The surveys were conducted using a DJI Mavic 3T Enterprise, equipped with a DJI RTK module and a DJI D-RTK 2 mobile station for GNSS base-station support. The Mavic 3T features a 48-megapixel RGB camera with a 24 mm focal length and a 640 × 512-pixel thermal camera with a 40 mm focal length. The drone was manually controlled to optimize the capture of surface temperatures across wide sections of the Shár Shaw Tagà River, recording both TIR and RGB videos simultaneously. Flight altitudes ranged from 5 to 20 m above ground level with near-nadir angles to reduce geometric distortion and minimize emissivity-related error (Torgersen et al., 2001; Dugdale et al., 2016). The survey began

157 180 m upstream of the N1 subsection and ended 800 m downstream of the N2 subsection (Fig. 2).

The TIR video was visually analyzed to identify cold water emergence zones using two criteria: 1) a clear contrast between the dominant stream surface temperature and the suspected exfiltration area, with an area larger than 10 cm², and 2) the presence of a turbulent mixing zone at least 1 m in length immediately downstream of the suspected area (flight data and information are available as Supplemental Material in Charonnat and Baraer, 2025). Absolute temperatures were not derived due to the absence of a calibrated color scale in the TIR video; instead, detection relied on qualitative identification of relative temperature differences appearing as visual color contrasts in the TIR video—typically, colder areas appeared as blue-toned patches compared to the green-toned stream and red-toned sunlit boulders.

When both criteria were met, the RGB video was used for confirmation. The Shár Shaw Tagà River, originating from glacial melt, has a substantial suspended sediment load, whereas groundwater is nearly free of suspended sediments. This contrast is visible in the RGB video frames. The observed thermal contrasts were consistent with previously measured field temperature differences between springs and stream water, typically >2°C and <6°C (Table S1) and exceeded the uncertainty range of uncorrected thermal imagery under field conditions (Zappa and Jessup, 1998). Finally, images of confirmed cold-water emergence zones were extracted from the videos for size evaluation.

# 3.1.2 TL monitoring

Three RGB timelapse (TL) cameras, designated TL1, TL2 and TL3, were installed along the right bank of the Shár Shaw Tagà River (TL1 and TL2: 61°5'26" N, 139°7'34" W; TL3: 61°5'12" N, 139°7'13" W; Fig. 2). TL1, installed in 2018, monitored the outwash plain immediately downstream of RG-A1. In 2019, TL2 was added adjacent to TL1, extending coverage from the upper margin of TL1's field of view to the outlet of the N2 subsection of the Shár Shaw Tagà River. Finally, TLC3 was added in 2021 on the bedrock outcrop, oriented toward the N1 subsection, with the upstream outwash plain in the background. All

cameras were configured to capture four images daily at 8:00, 11:00, 13:00, and 16:00. Visual analysis of the TL imagery involved identifying the origins of surface overflow within the riverbed and on the developing aufeis, as well as documenting their occurrence throughout the winter, following the protocol of Chesnokova et al. (2020). Monitoring these overflow events enabled the identification and spatial localization of groundwater outflow points.

#### 3.1.3 Radon activities measurements

- Radon (222Rn) serves as a natural tracer to detect groundwater exfiltration in streams (Cartwright and Hofmann, 2016). In June
- 2023, in situ radon activities were measured at two springs exhibiting the most visible discharge within the N1 subsection: S-
- 185 RG8, at the RG-A1's front, and S-RG9A, on the opposite talus slope (Fig. 2). Radon activities were also measured in the Shár
- Shaw Tagà River at the upstream and downstream ends of the N1 subsection (points S-RUP and S-R1, respectively). A portable
- 187 RAD7 Radon Monitor (Durridge) was used, coupled with the Rad Aqua accessory (Durridge) for radon degassing. Results are
- 188 reported in Bq m<sup>-3</sup>.

182

189

190

197

#### 3.2 Physico-hydrochemical characterisation

# 3.2.1 Sampling and field measurements

- 191 Physico-hydrochemical characterisation was undertaken over three campaigns to capture different hydrological conditions:
- June 2022, August 2022, and June 2023. The June 2022 campaign coincided with the melt of a late and substantial snowpack.
- 193 The August 2022 campaign took place when glacial ablation was at its peak. The June 2023 campaign was conducted following
- a winter with reduced snowpack and early snowmelt, after the primary snowmelt phase but before summer glacial ablation
- 195 commenced, while glaciers remained snow-covered. The three campaigns targeted both the Shár Shaw Tagà River and low-
- discharge springs along the front of RG-A1 to investigate subsurface connections between the rock glacier and the riverbed
- hypothesized to be drained by RG-A1 and therefore potentially contributing to the springs. In these areas, all flowing waters

(Fig. 2). Additional sites were selected in the proglacial field and in the ice-debris complex of the G-B1 subcatchment,

- 199 were systematically inventoried and sampled. Samples were categorized into four types (Table A1): glacial outlets from the
- G-B1 snout (S-GL#), streams in the ice-debris complex located between the G-B1 snout and RG-A1 (S-IDC#), springs at the
- 201 RG-A1 front and opposite talus (S-RG#), and Shár Shaw Tagà River (S-R#). When possible, sites were sampled multiple times
- within each campaign to account for diurnal fluctuations in physicochemical parameters.
- The physico-chemical characterization focuses on natural tracers' analysis for deciphering the origins of the groundwater
- outflows. Major and minor ions (Ca<sup>2+</sup>, Mg<sup>2+</sup>, Na<sup>+</sup>, Cl<sup>-</sup>, SO<sub>4</sub><sup>2-</sup>, K<sup>+</sup> and F<sup>-</sup>) were selected for the analysis as their concentrations
- in water are related to the groundwater residence time and pathways. The natural tracers' analysis includes water stable isotopes
- too. Field measurements comprehended in situ pH, electrical conductivity (EC, corrected to 25 °C, expressed in µS cm<sup>-1</sup>), and
- water temperature (°C), adding information about groundwater residence time and the presence of frozen content adjacent to

208 groundwater pathways. Measurements for pH, EC and water temperature were taken at each site using a calibrated Hanna HI 209 98195 multiparameter meter. 210 Water sampling followed a synoptic approach for cycles of 1-2 days, avoiding precipitation periods (e.g. Baraer et al., 2009). 211 Water samples were filtered using 0.45 um syringe filters and collected in 50 mL HDPE bottles, rinsed three times prior to 212 sampling. Not all sites were sampled at each campaign (Table A1), due to various factors (e.g., no flow or safety concerns 213 related to snow cover and rockfalls). Samples for major ion analysis were stored in a dark environment at 4 °C until analysis. 214 Major ions and minor ions were analyzed at the LG2 laboratory, École de technologie supérieure (ÉTS), Montreal, Canada. 215 Cation concentrations were measured using an inductively coupled plasma optical emission spectrometer (5110 ICP-OES. 216 Agilent), and anion concentrations were measured with an ion chromatograph (Dionex ED50, Thermo Fisher Scientific). 217 Bicarbonate (HCO<sub>3</sub><sup>-</sup>) concentrations were calculated from the charge balance equation, and total dissolved solids (TDS) were 218 derived from the sum of ion concentrations. Stable isotopic composition of the water molecule ( $\delta^{18}$ O and  $\delta^{2}$ H) was measured using a cavity ringdown spectrometer (Picarro L2130-i) at ÉTS, Montreal, Canada, expressed in % relative to Vienna Standard 219 220 Mean Ocean Water (VSMOW). Internal reference waters were used for normalization after every three analysis. Results were 221 interpreted following the methodology of Baraer et al. (2015). The absolute values of water temperature and EC measured in 222 situ were considered for tracers while means and ranges were used to assess the diversity in physico-chemical composition

223224

225

226

227

228

229

230

231

232

233

234

235

#### 3.2.2 Principal Component Analysis and clustering

among the samples for Principal Component analysis (PCA).

set of independent variables: water temperature, δ<sup>18</sup>O, Na<sup>+</sup>, Mg<sup>2+</sup>, Ca<sup>2+</sup>, and SO<sub>4</sub><sup>2-</sup>. These major ions were selected as they exhibited concentrations above the detection limit in more than 95 % of the samples. Principal components explaining at least 90 % of the total variance were retained for further analysis to ensure the robustness of the PCA.

After conducting PCA, clustering analysis was performed using the k-means algorithm for each campaign (Lloyd, 1982; MacQueen, 1967). This analysis was based on the sample scores derived from the selected principal components. The maximum number of clusters was set at 25 % of the total number of samples for each campaign, which corresponded to 5, 9 and 7 for the campaigns of June 2022, August 2022, and June 2023, respectively. The algorithm determined the resulting clusters were by associating samples with dominant combinations of variables, thereby highlighting inherent patterns within

Principal Component Analysis (PCA) was used to classify the origins of the sampled water and to identify sample groups that

influence the chemistry of the Shár Shaw Tagà River. For each of the three sampling campaigns, PCA was performed using a

236237

the dataset.

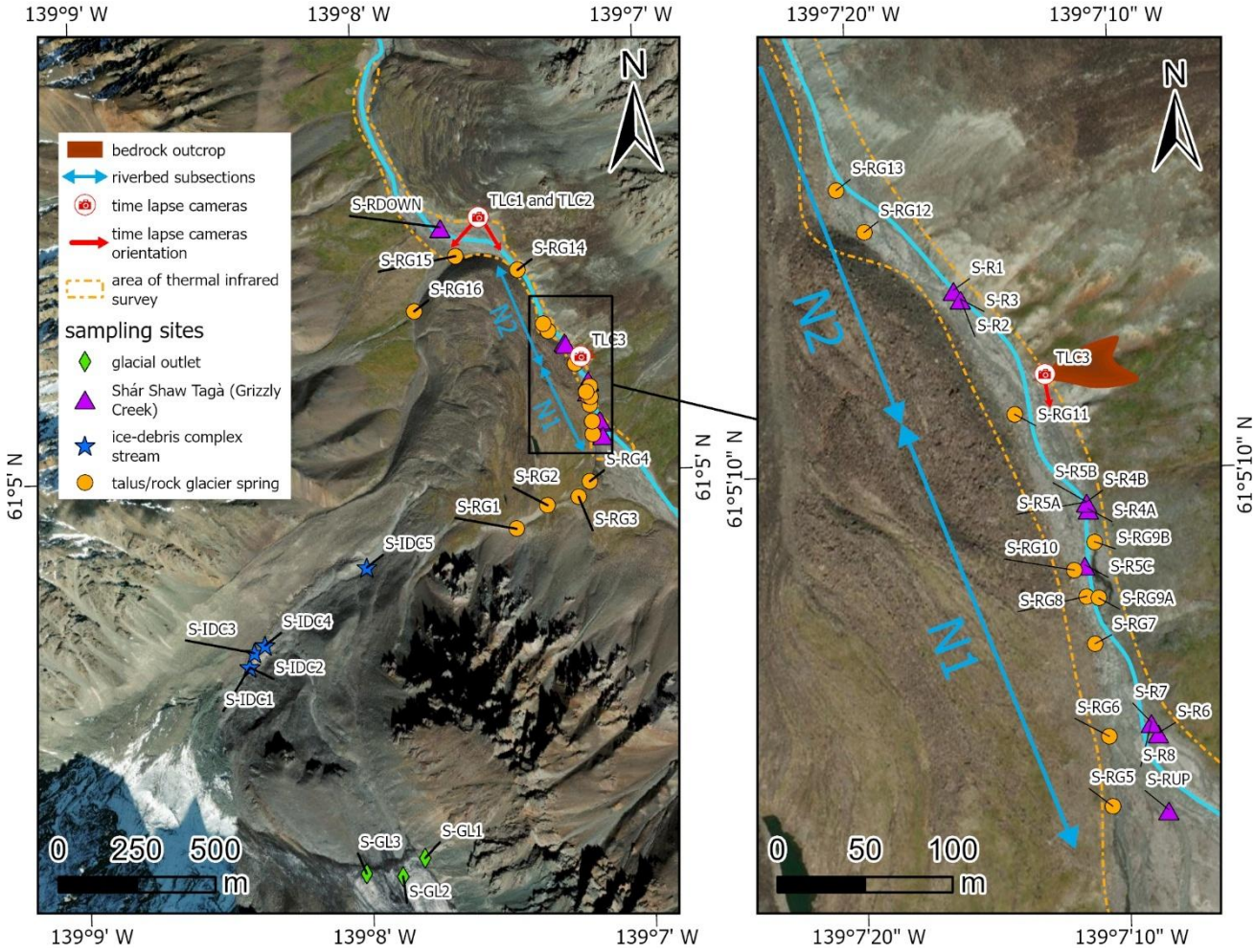


Fig. 2: Extent of the TIR survey and locations of sampling sites and TL cameras. Panel (a) corresponds to the study area, while panel (b) provides a zoom-in of panel (a). A bedrock outcrop on the talus slope opposite to RG-A1 marks the division of the Shár Shaw Tagà River's "narrow section" into two subsections, N1 and N2, as shown on the map. The spring locations represent the outflow points observed during the August 2022 campaign, though their positions may vary depending on hydro-meteorological conditions. Basemap credits: Esri.

#### 4. Results

#### 4.1 Monitoring and surveying of groundwater exfiltration

# 4.1.1 TIR survey

The TIR survey identified cold-water emergence zones in the downstream outwash plain and within the N1 subsection of the Shár Shaw Tagà River's "narrow section". Emergence zones from the left bank were labeled TIR-L#, and those from the right bank were labeled TIR-R#. In the imagery, these zones appeared as distinct color contrasts separating warmer surface waters

from colder emergences (Fig. 3a). At each site, the mixing plumes were mapped. In the most prominent emergence zones (plumes > 2 m in length), the visible video footage also showed clearer water, which provided additional confirmation of groundwater emergence (Fig. 3b).

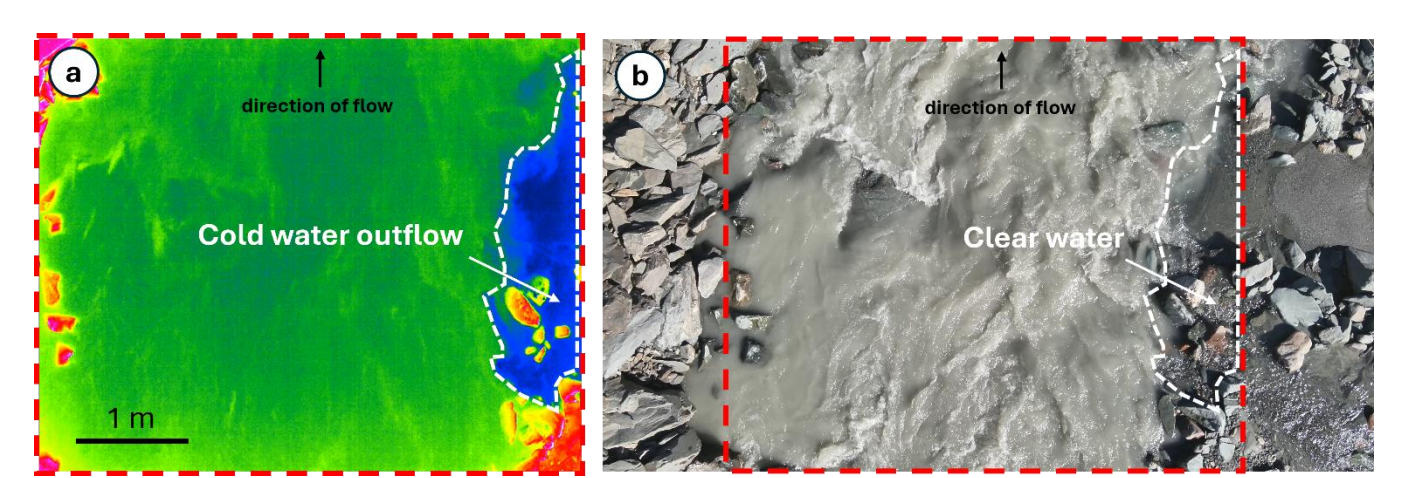


Fig. 3: (a) TIR capture showing cold groundwater emergence (in blue, delimited by the dashed white line), mixing with the warmer waters of the Shár Shaw Tagà River (in green) at the TIR-R2 location. Note that the video does not provide a color scale. (b) RGB image capture showing clear water flowing into the Shár Shaw Tagà River, which is characterized by a significant sediment load at the TIR-R2 location. The cold emergence zone detected with TIR is delimited by the dashed white line. The extent of the TIR capture is indicated by the dashed red line. Flight data and information can be accessed as Supplemental Material in Charonnat and Baraer (2025).

The TIR survey detected four cold emergence zones in the outwash plain downstream of RG-A1 (Fig. 4). Two cold emergence zones were identified on the left bank: one was observed to be associated with meltwater originating from a snow patch at the front of RG-A1, and the other was observed to be from a persistent snow patch on the west flank of the valley. The other two cold emergence zones were located on the right bank, originating from the middle of the outwash plain near the front of RG-B2. These four cold emergence zones are considered not fed by RG-A1, as they originate from snow patches or from the right bank and could not be related to any sampled spring.

Within the "narrow section", eight cold-water emergence zones were identified in the N1 subsection on the left bank of the main channel, and six on the right bank (Fig. 4). No cold-water emergence zone was detected in the N2 subsection. The furthest downstream cold emergence zone in the N1 subsection (TIR-L8) is located just a few meters upstream of the bedrock outcrop. Cold emergence zones on the left bank are generally smaller, with plume lengths ranging from 1 to 6 m, four of these less than 2 m long. In contrast, cold emergence zones on the right bank are larger, with plume lengths ranging from 5 to 14 m, and four exceed 10 m in length.

Of the six cold emergence zones identified on the right bank of the N1 subsection, two were located within a few meters of springs sampled in 2022 and 2023 (TIR-R2 and TIR-R3 can be associated to S-RG9A and S-RG9B, respectively). On the left bank, no cold emergence zone was detected in 2024 directly at the position of springs sampled in 2022 and 2023. However, as noted in Sect. 2, the outflow positions of springs on the left side of the river can shift 10–20 m downstream of the RG-A1 front, depending on river level and meteorological conditions. During the 2024 TIR survey, such conditions prevailed, and cold emergence zones were detected 20 m downstream of springs sampled in 2022 and 2023. Accordingly, cold emergence zones TIR-L1, TIR-L2, and TIR-L8 can be linked to springs S-RG8, S-RG10, and S-RG11, respectively (Fig. 4).

Overall, the drone-based TIR survey revealed a high density of cold water emergence zones along both the left and right banks of the N1 subsection, upstream of the bedrock outcrop. These zones, connected to springs sampled in 2022 and 2023, delineate a significant area of groundwater exfiltration within the upstream half of the "narrow section" of the Shár Shaw Tagà River,

139°7'50" W 139°7'40" W 139°7'30" W 139°7'20" W 139°7'10" W area of thermal infrared survey 61°5'30" N stream riverbed subsections cold water streams TIR+L10 cold outflows from left TIR-L9 cold outflows from right talus/rock glacier spring TIR-R7 bedrock outcrop snow patch 61°5'20" N 61°5'20" TIR-L8 TIR-R6 TIR+L6 TIR=L4 TIR-R4 TIR-L5 TIR-L2-TIR-R3 TIR-L1 TITR-R1 TIR-R2 61°5' N S-RG7 100 200 139°7 50" W 139°7<sup>1</sup>40" W 139°7'30" W 139°7 20" W 139°7 10" W

where flow is constrained by RG-A1 rock glacier.

275

276

277

278

279

280

281

282

283

284

285

286

287

# 4.1.2 TL monitoring

Over the 2018-2021 period, TL1 monitored aufeis formation during the winters of 2018-2019 and 2019-2020 (Fig. 5). No aufeis formation was observed during the winter of 2020-2021. The onset of aufeis development varied between the two winters. In 2018-2019, it began in early November and continued to develop throughout the winter season, whereas in 2019-2020, it started in February and progressed through February and March (Fig. 5). The development of the aufeis in both winters occurred in phases characterized by multiple flood events. Visible ablation of the aufeis began in May, with complete melt occurring by June in both 2019 and 2020. The aufeis that formed during the winters of 2018-2019 and 2019-2020 spanned the entire width of the river, from the RG-A1 front to the RG-B2 front.

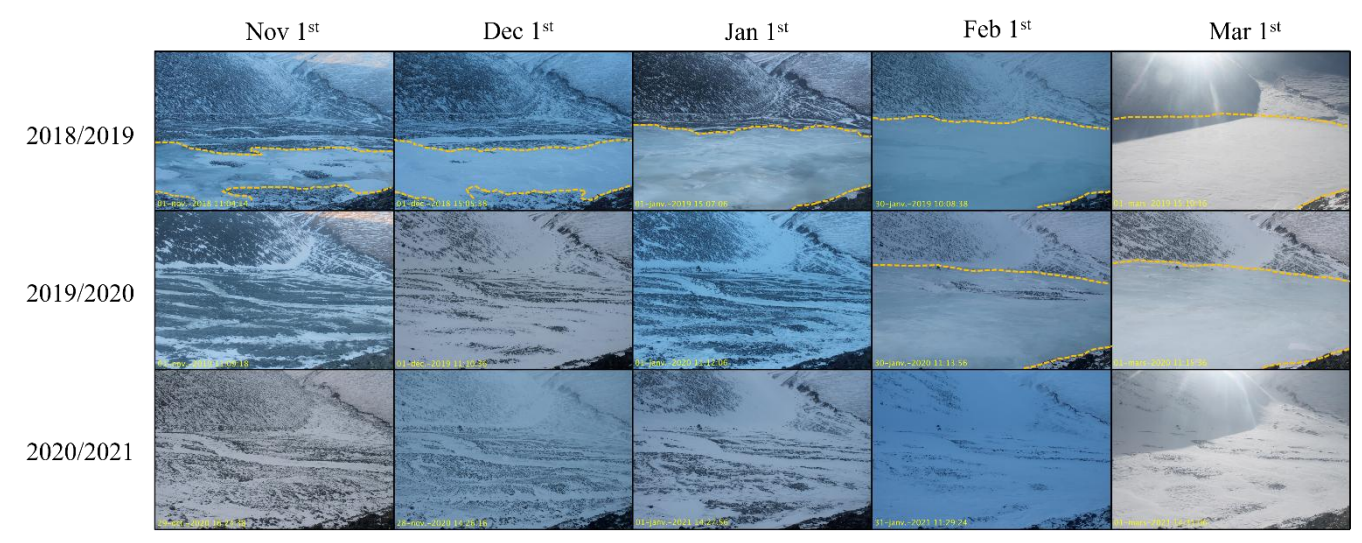


Fig. 5: Monthly timelapse images captured by TL1 of the aufeis from November 1st to March 1st during the winters of 2018-2019, 2019-2020, and 2020-2021. The yellow dashed line indicates the extent of the aufeis in each image when visible. The timelapse images were selected targeting the closest to the first day of each month, with consideration given to image quality. Note that no aufeis formation occurred during the 2020-2021 winter.

TL2, installed in 2019 next to TL1 and oriented towards the aufeis upstream section, recorded the formation of the aufeis in the winter of 2019-2020 and its absence during 2020-2021. In the winter of 2020, TL2 captured reflections of liquid water and/or ice at the end of the N2 subsection (Fig. 6a and 6b). In subsequent days, the aufeis was observed to form in the downstream outwash plain, starting from the end of the N2 subsection too.

TL3, installed in 2021 to monitor surface outflow in the N1 subsection, showed reflections of liquid water and/or ice from the entrance of the N1 subsection (Fig. 6c), while the upstream outwash plain remained without any visible surface outflow. These observations indicate that the liquid water available in winter to supply the aufeis could originate from the "narrow section"

between the upstream and the downstream outwash plains. The only winter during which TLC3 was installed to monitor surface flow in the "narrow section" coincided with the sole winter in which no aufeis developed in the downstream outwash plain. This observation suggests that surface flow in this section may play a more significant role in other years.









Fig. 6: Winter outflows in the downstream outwash plain (a, b) and in the N1 subsection (c), captured by TL2 on (a) 04/01/2020 at 08:00, (b) 08/01/2020 at 11:00, and TL3 on (c) 22/10/2021 at 13:00. The light in the raw images has been enhanced to improve picture quality. (a) and (b) are oriented towards the end of the N2 subsection and the entrance of the downstream outwash plain, while (c) is oriented towards the N1 subsection and the upstream outwash plain in the background. (a) At 8:00 on 04/01/2020, the aufeis has not yet formed, but reflections of ice and/or liquid water are visible at the end of the N2 subsection, during a time when the Shár Shaw Tagà River is dry. (b) At 11:00 on 08/01/2020, the aufeis has started to form in the outwash plain, extending from the end of the N2 subsection. (c) At 13:00 on 22/10/2021, surface outflow is visible from the entrance of the N1 subsection, but no outflow is visible in the upstream outwash plain in the background.

The monitoring of the aufeis provides evidence of overflow events during late fall and winter, particularly in the 2018-2019 and 2019-2020 periods. The continuous development of aufeis throughout winter, along with its large spatial extent, indicates the presence of a significant and stable water source. The formation of the aufeis is attributed to groundwater outflow from the "narrow section" of the Shár Shaw Tagà River, as the river runs dry in winter and surface outflow is visible from the N1 subsection. This finding aligns with the high density of springs inventoried along the N1 subsection with the TIR imagery.

#### 4.1.3 Radon activities measurements

In June 2023, while the Shár Shaw Tagà River level was lower than in previous years for the same period,  $^{222}$ Rn activities were similar at S-RG8 and S-RG9A, ranging from  $10.17 \times 10^3 \pm 0.22 \times 10^3$  Bq m<sup>-3</sup> to  $10.85 \times 10^3 \pm 0.19 \times 10^3$  Bq m<sup>-3</sup> (Fig. 7). These springs are located along the N1 subsection of the river, at the left and the right of the stream, respectively. In contrast, the Shár Shaw Tagà River at the upstream end of the N1 subsection (S-RUP) exhibited low activities  $(0.36 \times 10^3 \pm 0.06 \times 10^3 \text{ Bq m}^{-3})$ , while the downstream end of N1 (S-R1) showed significantly higher activities  $(5.46 \times 10^3 \pm 0.14 \times 10^3 \text{ Bq m}^{-3})$ . These results clearly indicate groundwater input to the Shár Shaw Tagà River in the N1 subsection, where S-RG8 and S-RG9A are located.

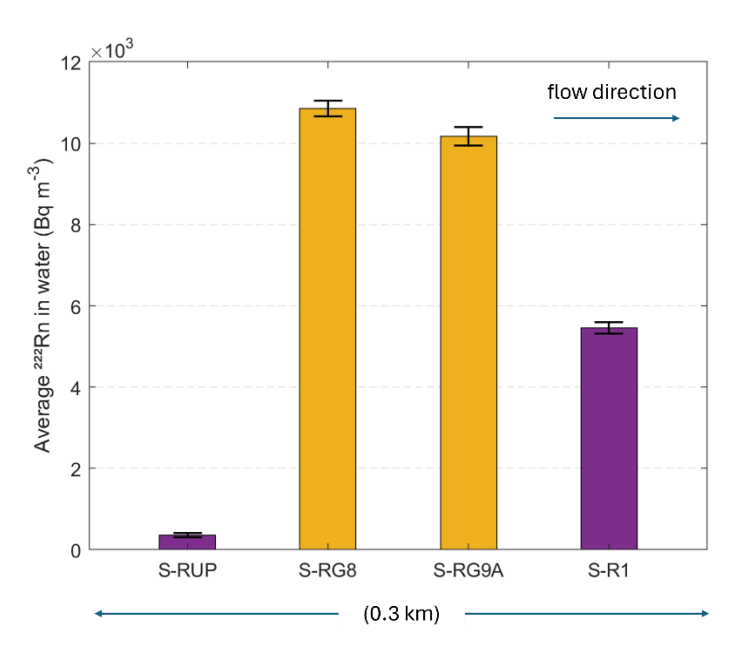


Fig. 7: <sup>222</sup>Rn activities measured with a portable RAD7 Radon Monitor (Durridge) in June 2023. Data were collected at springs S-RG8 and S-RG9A (orange) and along the Shár Shaw Tagà river at upstream (S-RUP) and downstream (S-R1) sites (purple). The bars are arranged from left to right in spatial sequence from upstream to downstream. The error bars represent the uncertainties in the radon activity measurements.

#### 4.2 Physico-hydrochemical characterization

# 4.2.1 Sampling and field measurements

The mean water temperature of springs at the front of RG-A1 was 0.90 °C in June 2022, slightly colder than in August 2022 and June 2023, respectively exhibiting mean temperatures of 1.38 °C and 1.40 °C (Table S1). The colder conditions in June 2022 likely reflect recent snowmelt, whereas no snow cover remained at lower elevations during August 2022 and June 2023. Groundwater outflows with temperatures below 2 °C in late season are commonly interpreted as evidence of adjacent frozen material (Carturan et al., 2016; Frauenfelder et al., 1998; Haeberli, 1975; Scapozza, 2009). Accordingly, the cold temperatures measured in August 2022 in the springs at the RG-A1's front inform on persistence of frozen content nearthe front of the rock glacier.

High EC ranges (respectively 439.10 μS cm<sup>-1</sup> and 546.72 μS cm<sup>-1</sup> in June and August 2022) underscore the heterogeneous behaviour of the sampled springs. This apparent diversity in physico-chemical composition provides the basis for applying PCA to cluster springs according to their properties.

#### 4.2.2 Principal Component Analysis and clustering

#### Samples collected in June 2022

357

358

376

359 Principal Component (PC) 1 accounts for 60.96 % of the variance in the dataset and primarily reflects the influence of ionic 360 elements, with PC scores ranging from 0.47 to 0.50 (Fig. 8a). PC2 and PC3, explaining 18.29 % and 14.10 % of the variance, 361 respectively, exhibit contrasting associations with the  $\delta^{18}$ O ratio and temperature. PC2 displays a strong positive correlation 362 with the  $\delta^{18}$ O ratio (0.73) and a negative correlation with temperature (-0.67), whereas PC3 shows positive correlations with 363  $\delta^{18}O$  (0.62) and temperature (0.71). 364 Clustering analysis based on PCA reveals two distinct clusters among the June 2022 samples (Fig. 8b). Cluster 1 comprises 365 17 samples characterized by low concentrations of mineral elements (Fig. 8c), with total dissolved solids (TDS) concentrations 366 ranging from 28 to 100 mg L<sup>-1</sup>. In contrast, Cluster 2 includes samples S-RG4, S-RG5, and S-RG8, which show elevated TDS 367 values (90 to 269 mg L<sup>-1</sup>). S-RG5 is grouped within Cluster 2 primarily due to its elevated water temperature, while its other 368 physico-chemical characteristics closely resemble those of the Cluster 1 samples. With the exception of S-RUP, S-RG4, and 369 S-RG15, which record warmer temperatures from 1.43 to 3.19 °C, the remaining 16 samples in the June 2022 dataset exhibit 370 colder temperatures, ranging from 0.03 °C to 0.67 °C (Fig. 8c). The most enriched samples are S-IDC2, S-RG7, S-RG8, and 371 S-RG10, with  $\delta^{18}$ O values between -23 % and -22.6 % vs. VSMOW in  $\delta^{18}$ O (Fig. 8d). 372 In June 2022, 17 springs (Cluster 1) were supplied by recent snowmelt, as indicated by low concentrations of mineral elements 373 and cold temperatures. In contrast, S-RG8 and S-RG4 (Cluster 2) were supplied by groundwater, as evidenced by their higher 374 concentrations of mineral elements. The comparatively enriched  $\delta^{18}$ O values of S-IDC2, S-RG7, S-RG8, and S-RG10 may indicate mixing with a source other than snowmelt, such as glacial meltwater, as they approach the  $\delta^{18}O$  values measured in 375

glacial meltwater samples collected in August 2022 (see following paragraph).

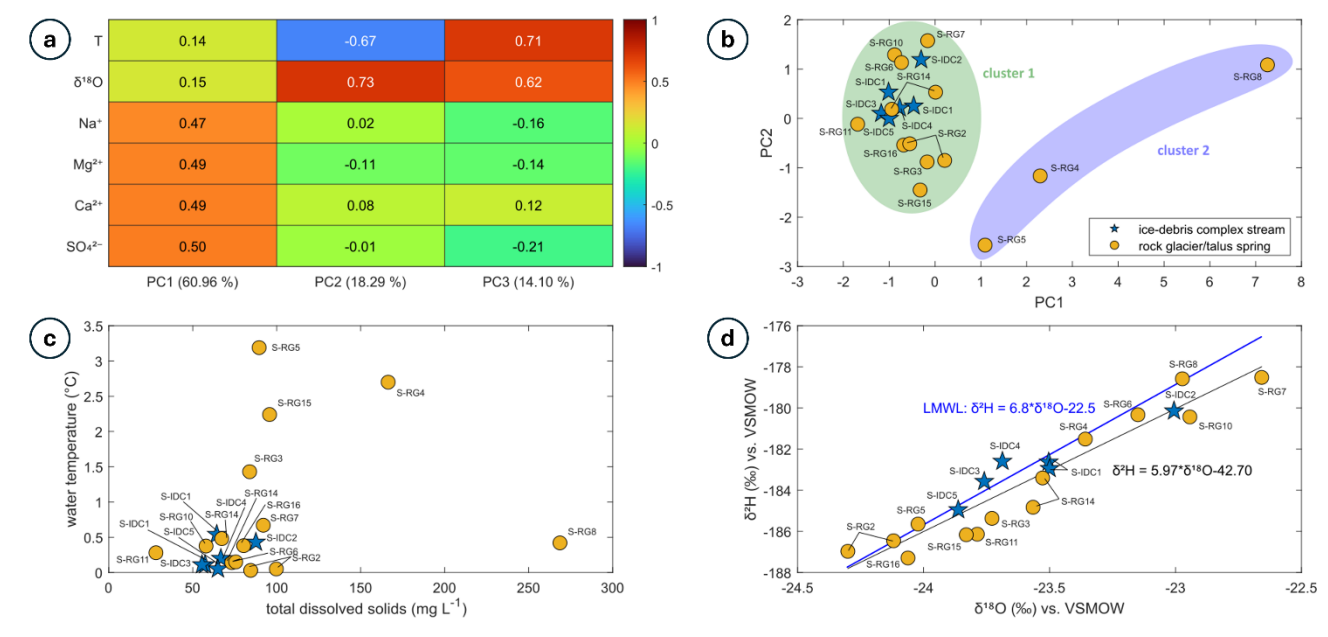


Fig. 8: (a) PCA scores for June 2022 samples. The explained variance for each PC is indicated in the legend of the horizontal axis. (b) Distribution of clusters formed from June 2022 samples following PCA and k-means clustering. Symbols represent different sample types, and ellipses illustrate the distribution of each cluster. (c) Distribution of total dissolved solids (TDS) concentrations and water temperature for the June 2022 samples. (d) Isotopic composition of the June 2022 samples.

#### Samples collected in August 2022

PC1 accounts for 60.57 % of the variance in the dataset and is strongly influenced by solute concentrations, with PC scores ranging from 0.47 to 0.48 (Fig. 9a). PC2, which explains 22.34 % of the variance, reflects opposing influences of temperature (0.68) and isotopic composition (-0.63). PC3, accounting for 9.01 % of the variance, shows joint positive correlations with both temperature (0.71) and isotopic composition (0.63).

Clustering analysis clearly distinguishes different sample types, forming 9 clusters, the maximum achievable based on the parametrization (Fig. 9b). Cluster 3 consists of glacial outlet samples, characterized by low solute concentrations (16 to 38 mg L<sup>-1</sup> in TDS), cold temperatures (0.06 to 0.07 °C), and depleted isotopic compositions (-21.6 to -22 ‰ vs. VSMOW in  $\delta^{18}$ O) as seen in Figs. 9c and 9d. Clusters 5 and 6 comprise Shár Shaw Tagà River samples, with warmer temperatures (3.47 °C to 6.26 °C), higher solute concentrations (88 to 238 mg L<sup>-1</sup> in TDS), and depleted isotopic compositions (-21.8 to -22.2 ‰ vs. VSMOW in  $\delta^{18}$ O). The distinction between these clusters may be attributed to variations in the glacial regime diurnal cycle and weather conditions based on sampling times. Clusters 4 and 8 include samples from springs near the upper end of the rock glacier front and at the transition area with the ice-debris complex (e.g., S-IDC5, S-RG1, S-RG2). As shown in Figs. 9c and 9d, these springs display high concentrations of mineral elements (209 to 304 mg L<sup>-1</sup> in TDS) and enriched isotopic compositions (-20.6 to -20.9 ‰ vs. VSMOW in  $\delta^{18}$ O). Clusters 2 and 9 are represented by springs S-RG7, S-RG8, S-RG9A, and S-IDC1, which

exhibit high but narrow ranges of solute concentrations (282 to 309 mg L<sup>-1</sup> in TDS) and more depleted isotopic compositions (-21.6 to -21.8 % vs. VSMOW in  $\delta^{18}$ O), as shown in Fig. 9d. Clusters 1 and 7 include other springs from the N1 subsection of the Shár Shaw Tagà River, which are characterized by low solute concentrations (111 to 162 mg L<sup>-1</sup> in TDS) and enriched isotopic compositions (-20.4 to -20.9 % vs. VSMOW in  $\delta^{18}$ O). Fig. 9d clearly distinguishes samples with depleted isotopic compositions (below -21.5 % vs. VSMOW in  $\delta^{18}$ O) from those with enriched compositions (above -20.9 % vs. VSMOW in  $\delta^{18}$ O).

In late summer, the hydrochemical signatures of the springs show significant contrasts, with a high number of clusters. However, springs S-RG7, S-RG8, and S-RG9A share isotopic signatures similar to glacial meltwater from S-G1, S-G2, S-G3, and Shár Shaw Tagà River samples, indicating a glacial input. Despite being located on opposite sides of the river, these springs cluster together, contrasting with the other springs. 25 rock glacier spring samples show cold temperatures (< 2 °C; Fig. 9c). Other springs appear to originate from summer precipitation, as indicated by their enriched isotopic signatures. Among these, some exhibit short residence times, reflected by low solute concentrations (S-RG5, S-RG6, S-RG12, S-RG13, and S-RG14), whereas others show longer residence times, reflected by higher solute concentrations (S-RG1, S-RG2, and S-IDC5).

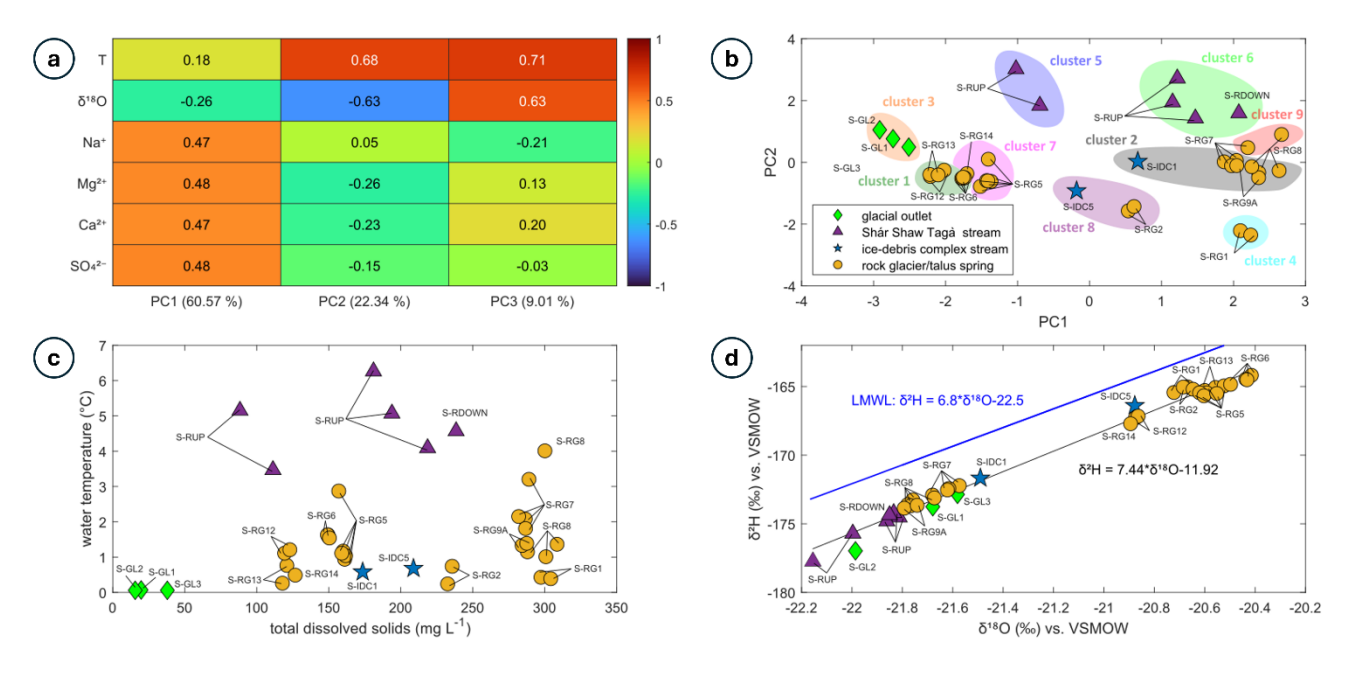


Fig. 9: (a) PCA scores for August 2022 samples. The explained variance for each PC is indicated in the legend of the horizontal axis. (b) Distribution of clusters formed from August 2022 samples following PCA and k-means clustering. Symbols represent different sample types, and ellipses illustrate the distribution of each cluster. (c) Distribution of total dissolved solids (TDS) concentrations and water temperature for the August 2022 samples. (d) Isotopic composition of the August 2022 samples.

# Samples collected in June 2023

419 420 PCA conducted on samples collected in June 2023 revealed that PC1 accounts for 68.79 % of the variance (Fig. 10a), primarily 421 driven by solute concentrations (PC scores ranging from 0.40 to 0.48), PC2 and PC3 explain 15.54 % and 10.43 % of the 422 variance, respectively. PC2 is mainly influenced by water temperature (0.88), while PC3 is dominated by isotopic composition 423 (0.86).424 The glacier outlet samples form a distinct cluster, labeled as Cluster 3 (Fig. 10b). The remaining samples are divided into two 425 clusters, with a clear distinction based on the maximum number of clusters (5). Cluster 1 consists solely of Shár Shaw Tagà 426 River samples from the upstream part of the N1 subsection. Cluster 2 includes spring samples and Shár Shaw Tagà River 427 samples collected in the downstream part of the N1 subsection. River samples from the downstream N1 subsection and spring samples exhibit higher solute concentrations (from 121 to 147 mg L<sup>-1</sup> in TDS) and colder temperatures (from 0.7 to 4 °C, with 428 429 14 out of 16 samples < 2 °C) compared to the upstream N1 samples, which have lower solute concentrations (87 to 125 mg L 430 1) and warmer temperatures (5.3 to 9.5 °C; Fig. 10c). The isotopic composition is generally more enriched for the upstream 431 N1 river samples than for the downstream N1 river and spring samples (Fig. 10d). The isotopic composition of one of the two 432 glacial water samples from G-B1 (sample S-GL1) is similar to the composition from the Shár Shaw Tagà River in upstream 433 N1 (water flowing from G-A1). However, the second S-GL1 sample shows a much more enriched isotopic composition, due to a two-day interval between the respective samplings. The most enriched sample (-21.2 % vs. VSMOW in  $\delta^{18}$ O and -165.4 434 435 % vs. VSMOW in  $\delta^2$ H) was taken first, when the G-B1 glacier was still snow-covered. The most depleted sample (-22.4 %436 vs. VSMOW in  $\delta^{18}$ O and -173.6 % vs. VSMOW in  $\delta^{2}$ H) was taken two days later, following significant snowmelt cover on G-B1 and the initiation of glacial melt. 438 439

437

The springs located on opposite sides of the river along the N1 subsection cluster together (Cluster 2) and exhibit close hydrochemical signatures, similar to what was observed in August 2022. By distinguishing between two clusters, the PCA 440 highlights the important influence of these springs on the Shár Shaw Tagà River. Their outflows significantly lower the water 441 temperature and increase solute concentrations in the river.

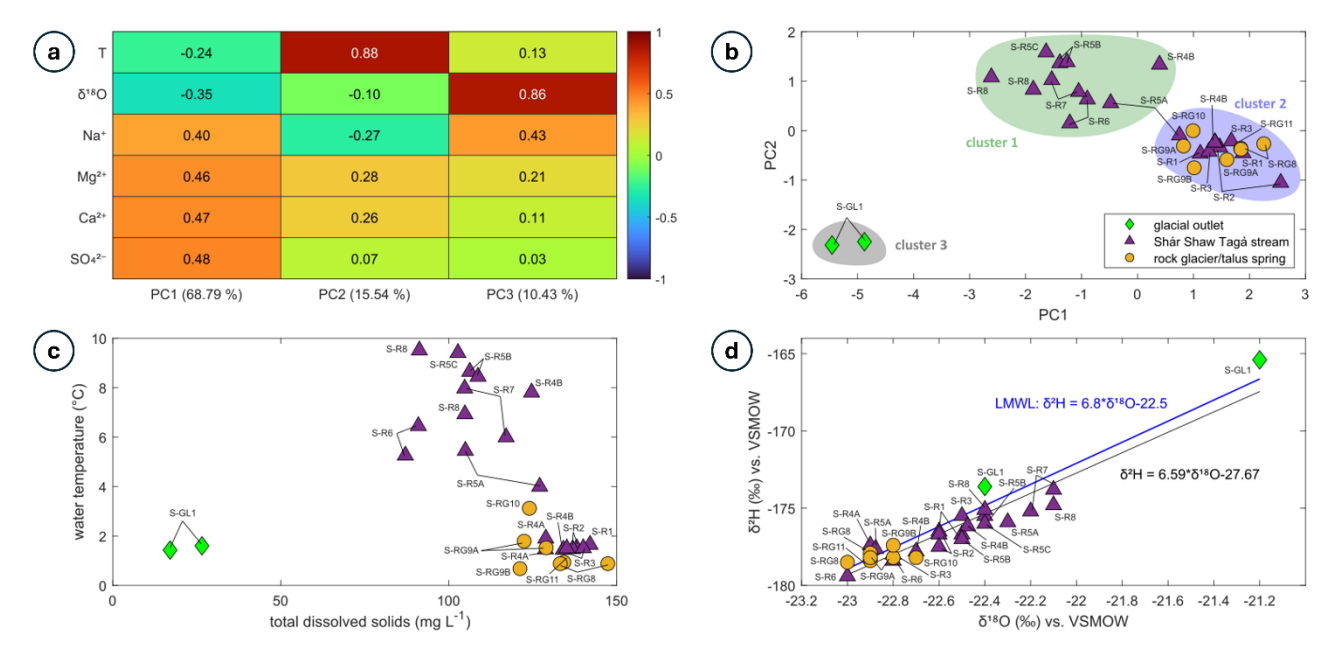


Fig. 10: (a) PCA scores for June 2023 samples. The explained variance for each PC is indicated in the legend of the horizontal axis. (b) Distribution of clusters formed from June 2023 following PCA and k-means clustering. Symbols represent different sample types, and ellipses illustrate the distribution of each cluster. (c) Distribution of total dissolved solids (TDS) concentrations and water temperature for the June 2023 samples. (d) Isotopic composition of the June 2023 samples.

## Synthesis of physico-hydrochemical characterisation

The springs surrounding RG-A1's front exhibit heterogeneous hydrochemical signatures, highlighting their connection to different drainage systems. A group of springs along the N1 subsection (S-RG7, S-RG8, and S-RG9A) cluster together in PCA and share high EC values, depleted isotopic compositions, high solute concentrations. Despite being located on opposite sides of the river, these three springs show striking similarities, suggesting a common origin. Their isotopic compositions are comparable to those of glacial meltwater sampled at the snout of G-B1 and in the Shár Shaw Tagà River, differing significantly from other springs along RG-A1's front. The other springs at the RG-A1's front exhibit diverse hydrochemical signatures under varying hydro-meteorological conditions. However, they exhibit signatures of recent precipitation, originating from snowmelt in the early season or rainfall in the late season. Variations in solute concentrations reveal both short and prolonged residence times among these springs, indicating distinct groundwater flow pathways. Most of the springs consistently exhibit cold temperatures, suggesting flow path adjacent to frozen content. During low-discharge periods, such as June 2023, the springs along the N1 subsection considerably increase downstream solute concentrations and radon activities in the Shár Shaw Tagà River, while their cold outflows reduce stream temperature.

### 5. Discussion

460

461

491

492

#### 5.1 Indirect influence of the rock glacier

- 462 The TIR survey, aufeis monitoring and radon activities measurements identified a major zone of groundwater emergence in 463 the N1 subsection of the Shár Shaw Tagà River, connected to springs both at the front of the rock glacier and on the opposite 464 talus slope. TL camera monitoring confirmed that this zone remains active during winter. Physico-hydrochemical 465 characterization indicates that springs on both banks of the N1 subsection share a glacial meltwater signature. No evidence 466 was found for outflow originating from the head of the rock glacier's subcatchment (fed by glaciers G-B1 and G-B2). 467 Furthermore, contributions from internal ice melt to rock glacier discharge are minimal and exert little influence on isotopic 468 concentrations (Croce and Milana, 2002; Krainer and Mostler, 2002; Krainer et al., 2007). 469 Thus, these springs do not represent outlets of the rock glacier's internal drainage system. Instead, their similar physico-470 hydrochemical composition indicate the emerging water originates from the same glacial source, which is coherent with field 471 observations. Located on opposite banks of the river, these springs are fed exclusively by upstream outwash plains of the main 472 Shár Shaw Tagà catchment. In June 2023, surface flow temporarily ceased upstream of the outwash plain, resuming only in 473 the N1 subsection via groundwater inflows. Together, these observations indicate that springs in the N1 subsection are not 474 sourced from the rock glacier, but are rather sustained by a shallow aguifer recharged by upstream glacial meltwater, potentially 475 infiltrating the riverbed or the glacier bed. 476 Parafluvial flow is common in outwash plains with coarse-grained unconsolidated sediments, occurring in river reaches where 477 water is lost before rejoining the river in gaining reaches (Cartwright and Hofmann, 2016). Such plains, often underlain by 478 bedrock, retain groundwater in the shallow subsurface and provide baseflow during low-discharge periods (Müller et al., 2024). 479 In this case, the parafluvial and shallow groundwater resurgence is visible during low-flow periods. The variable location of 480 the springs between sampling campaigns reflects the changes in stored groundwater volume in the alluvial aquifer. The lower 481 density of springs beyond the bedrock outcrop at the downstream end of the N1 subsection suggests a shallow bedrock interface 482 with limited groundwater flow capacity. 483 Cold temperatures in the springs of the N1 subsection indicate that outflows are cooled by adjacent frozen content, such as 484 massive ice or permafrost (e.g. Carturan et al., 2016). Frozen content has been confirmed within the rock glacier by Evin et al. 485 (1997), and is suspected within the talus slope, based on Scapozza (2015). Frozen material on both banks constrains the alluvial 486 aguifer, forcing groundwater to emerge through springs and cold-water upwellings. The narrowing of the riverbed by the 487 advancing rock glacier further enforces this constraint. Consequently, the resurgences in the N1 subsection can be explained 488 by the rock glacier's geomorphic properties: the combination of riverbed narrowing and obstruction by frozen content 489 constrains subsurface flow, demonstrating an indirect hydrological role through geomorphic control. 490
  - This indirect influence produces a high density of cold springs (< 2 °C) along the N1 subsection with distinct physicochemical signatures. The resurgences substantially affect downstream river composition and promote aufeis formation. Solute enrichment in these springs arises from water-rock interactions along groundwater flow paths, with prolonged residence time

facilitating the accumulation of dissolved solutes (Hem, 1985). Proximity to buried ground ice and permafrost within the rock glacier and opposite talus slope may further enhance the release of mineral elements through thermal erosion of the ice-sediment matrix (Jones et al., 2019). Physico-hydrochemical characterization from June 2023 demonstrates that, during dry periods, these springs notably increase solute concentrations and radon activities, while simultaneously cooling river water. The consequences of the rock glacier's indirect influence are comparable with the direct impact of rock glaciers outflows on the physicochemical characteristics of downstream surface waters, demonstrated in previous studies (e.g., Bearzot et al., 2023; Brighenti et al., 2023; Robinson et al., 2022; Wagner et al., 2021). Yet, our results indicate that rock glaciers can also exert this influence on riverbed systems primarily in an indirect manner, through their geomorphic and thermal properties—a mechanism not previously documented in the literature.

# 5.2 Direct influence of the rock glacier

493

494

495

496

497

498

499

500

501

502

503

504

505

506

507

508

509

510

511

512

513

514

515

516

517

518

519

520

521

The other springs emerging at the rock glacier front outside the N1 subsection, or within the N1 subsection but not forming a major groundwater emergence area, appear to be associated with the rock glacier's internal drainage system. These springs exhibit limited discharge and exert minimal influence on the riverbed. They are primarily sustained by snowmelt in early season and by summer precipitation later in the season, with little to no contribution from glacial melt, as indicated by the physico-hydrochemical characterization of samples collected in June 2022 and August 2022. In Canada, precipitation is typically enriched in heavy isotopes during the snow-free period and depleted during winter and spring (Gibson et al., 2020). Accordingly, the depleted isotopic compositions, low solute concentrations, and cold temperatures measured in early June 2022 point to a snowmelt origin, whereas the enriched isotopic compositions in August reflect a stronger rainfall influence. Thus, they are fed by rapid flow paths and respond to meteorological conditions. Variations in solute concentrations among these springs reflect differences in residence time, thereby indicating distinct flow pathways within the rock glacier. Some springs in the N1 subsection likely represent a mix of precipitation-fed and glacier-fed sources, with physicochemical parameters and clustering reflecting these dual contributions depending on hydro-meteorological conditions and timing. The behaviour and composition of these springs are consistent with observations from other rock glacier hydrology studies (e.g., Jones et al., 2019). Nevertheless, their influence on streamflow discharge and composition appears limited in the immediate vicinity of the rock glacier. Further work beyond the riverbed survey area would be required to locate outflows from the G-B1 and GB-2 subcatchments which could not be detected. The relatively minor impact of these direct outflows contrasts sharply with the substantial indirect influence exerted by resurgences geomorphically constrained by the rock glacier (Sect. 5.1).

# 5.3 Possible evolution of the rock glacier influence on catchment hydrology

be envisaged across different timescales when considering the role of ground ice in constraining the riverbed and driving groundwater resurgences. Frozen content is likely to persist in depositional landforms for an extended period, as residual ice has been detected in rock glaciers below the modeled elevation limit in multiple cases (e.g., Carturan et al., 2024; Colucci et al., 2019). Future hydrological conditions in alpine catchments are expected to feature a reduced contribution from glaciers, lower discharge and an increased contribution from groundwater and periglacial features to streamflow (Huss et al., 2017; Jones et al., 2019; Zierl and Bugmann, 2005). These conditions were observed during the June 2023 sampling campaign, which took place after the peak of snowmelt and prior to the peak of glacial ablation, resulting in a substantial influence of groundwater resurgences on the Shár Shaw Tagà River. A similar pattern may occur in the future, with rock glacier-driven groundwater outflows gaining importance in the Shár Shaw Tagà River.

However, ongoing cryosphere degradation under rising air temperatures may render this configuration transitory. Permafrost thaw within the rock glacier and the opposite talus slope will likely reduce geomorphic constraints on the riverbed and diminish obstruction of shallow groundwater flow. The dynamic and transient nature of flow paths across the rock glacier has been previously noted (Johnson, 1978). Furthermore, thermal and mechanical erosion induced by shallow groundwater flow could expand the parafluvial flow zone and create alternative subsurface pathways, reducing the hydrological discontinuity and

Predicting the future evolution of the system described in Sect. 5.1 and 5.2 is challenging. Nonetheless, several scenarios can

## 5.4 Limitations and perspectives

disruptive effects currently imposed by the rock glacier.

The physico-hydrochemical characterization in this study was based on three sampling campaigns conducted under varying hydro-meteorological conditions. These diverse settings posed several challenges for water sampling, including issues with accessibility, safety concerns, periods of no flow, and the need to prioritize specific areas. As a result, some sites could not be revisited during every campaign. Consequently, some sites could not be compared across campaigns, and their characterization can remain incomplete. Moreover, fluctuating weather conditions during a single campaign in proglacial environments likely contributed to variations in physicochemical parameters at some sites. When possible, multiple samples were taken at different times or on different days within the same campaign to minimize biases caused by diurnal and meteorological variations. This study demonstrates that the indirect hydrological influence of rock glaciers can exceed their direct influence. Future research could build on these findings by investigating the hydrological influences of other rock glaciers extending into valley floors to evaluate the representativeness of this case. Such studies would clarify whether similar patterns occur in different settings. Furthermore, monitoring and modelling of comparable configurations could improve predictions of how these systems may evolve and influence catchment hydrology under ongoing cryosphere degradation. The authors strongly encourage further works in this direction.

#### 6. Conclusions

The objective of this study was to simultaneously evaluate the direct and indirect influences of a rock glacier on the hydrology of an alpine riverbed. We aim to provide new insights into the hydrological processes and their evolution, focusing on both surface flow and shallow groundwater fluxes within the Shár Shaw Tagà subcatchment, Yukon, Canada.

We adopted a multi-method approach combining field observations, drone-based thermal infrared (TIR) surveys, aufeis monitoring and radon activities measurements to identify groundwater emergence zones, alongside physico-hydrochemical analyses of water sources. This methodology enabled us to distinguish contributions originating directly from the rock glacier from those sourced from a shallow aquifer recharged by upstream glacial meltwater.

Our results indicate that the indirect influence of the rock glacier on the riverbed system, through its geomorphic and thermal properties constraining subsurface flow, exerts a greater impact on discharge and water chemistry than direct contributions from the rock glacier. The dynamic landform functions as a structural constraint within the riverbed, forcing groundwater resurgence and substantially affecting downstream physicochemical properties and aufeis formation.

The presence of frozen content in the rock glacier and in the opposite talus slope is central to this indirect influence, modulating constraint on the alluvial aquifer and likely governing the evolution of these flows under ongoing deglaciation and permafrost thaw. Understanding this factor is therefore essential for anticipating changes in alpine hydrological systems under climate warming.

Our findings highlight that studies of rock glacier hydrology on catchments should account for indirect effects, which can surpass direct contributions and play a critical role in redistributing both surface and subsurface waters in alpine environments.

#### Appendix: Table A1

Sampling sites	Northing (UTM)	Easting (UTM)	Elevation (m a.s.l.)	Comments	Dates and times of sampling		
					June 2022	August 2022	June 2023
S-R1	6773938	601332	1738	Shár Shaw Tagà river (narrow section)	NV	NV	15/06/23 12:50 16/06/23 13:00
S-R2	6773933	601336	1739	Shár Shaw Tagà river (narrow section)	NV	NV	15/06/23 13:07 16/06/23 13:10
S-R3	6773933	601336	1739	Shár Shaw Tagà river (narrow section)	NV	NV	15/06/23 13:25 16/06/23 13:40

S-R4A	6773813	601409	1741	Shár Shaw Tagà river (narrow section)	NV	NV	15/06/23 13:50
S-R4B	6773817	601408	1746	Shár Shaw Tagà river (narrow section)	NV	NV	15/06/23 14:35 16/06/23 14:20
S-R5A	6773817	601408	1746	Shár Shaw Tagà river (narrow section)	NV	NV	15/06/23 14:40 16/06/23 15:10
S-R5B	6773817	601408	1746	Shár Shaw Tagà river (narrow section)	NV	NV	15/06/23 14:10 16/06/23 15:25
S-R5C	6773781	601407	1747	Shár Shaw Tagà river (narrow section)	NV	NV	16/06/23 14:45
S-R6	6773685	601449	1759	Shár Shaw Tagà river (narrow section)	NV	NV	15/06/23 16:40 16/06/23 15:45
S-R7	6773691	601445	1753	Shár Shaw Tagà river (narrow section)	NV	NV	15/06/23 16:50 16/06/23 16:00
S-R8	6773691	601445	1753	Shár Shaw Tagà river (narrow section)	NV	NV	15/06/23 17:00 16/06/23 16:10
S-RDOWN	6774302	600936	1687	Shár Shaw Tagà river (downstream floodplain)	NV	19/08/22 13:05	NV
S-RUP	6773641	601455	1749	Shár Shaw Tagà river (upstream floodplain)	NV	16/08/22 12:00 16/08/22 16:16 17/08/22 13:12 18/08/22 12:35 19/08/22 13:01	NV
S-GL1	6772289	600889	2083	stream at G-B1 snout	NV	18/08/22 18:36	19/06/23 14:35 21/06/23 12:05
S-GL2	6772230	600819	2109	stream at G-B1 snout	NV	18/08/22 18:06	NV
S-GL3	6772239	600703	2086	stream at G-B1 snout	NV	18/08/22 19:03	NV
S-IDC1	6772896	600330	1886	ice-debris complex stream	16/06/22 15:56 18/06/22 17:50	18/08/22 20:29	NV
S-IDC2	6772897	600330	1886	ice-debris complex stream	18/06/22 17:56	NV	NV
S-IDC3	6772943	600345	1891	ice-debris complex stream	16/06/22 15:37	NV	NV
S-IDC4	6772967	600379	1893	ice-debris complex stream	16/06/22 17:04	NV	NV

S-IDC5	6773216	600703	1860	ice-debris complex stream	16/06/22 17:40	18/08/22 20:55	NV
S-RG1	6773340	601180	1797	spring at RG-A1 front	NV	17/08/22 11:58 18/08/22 13:52	NV
S-RG2	6773415	601279	1780	spring at RG-A1 front	12/06/22 16:54 19/06/22 15:08	16/08/22 11:15 17/08/22 12:14	NF
S-RG3	6773442	601378	1770	spring at RG-A1 front	19/06/22 14:48	NF	NF
S-RG4	6773492	601414	1770	spring at RG-A1 front	19/06/22 13:52	NF	NF
S-RG5	6773643	601423	1770	spring at RG-A1 front	19/06/22 13:45	16/08/22 11:30 16/08/22 16:04 17/08/22 12:44 18/08/22 12:47 19/08/22 13:46	NV
S-RG6	6773683	601421	1758	spring at RG-A1 front	19/06/22 13:30	16/08/22 12:40 17/08/22 13:05 18/08/22 12:27 19/08/22 13:24	NV
S-RG7	6773736	601413	1746	spring at RG-A1 front	19/06/22 13:18	16/08/22 13:05 17/08/22 13:58 18/08/22 12:14 19/08/22 13:12	NV
S-RG8	6773763	601408	1744	spring at RG-A1 front	19/06/22 12:50	16/08/22 13:15 17/08/22 14:13 18/08/22 11:11 19/08/22 12:34	15/06/23 14:55 16/06/23 14:35
S-RG9A	6773762	601415	1752	spring flowing from talus opposite to RG-A1 front (right bank)	NV	16/08/22 12:13 17/08/22 13:29	15/06/23 14:55 16/06/23 14:25
S-RG9B	6773931	601335	1734	spring from talus opposite to RG-A1 front (right bank)	NV	NV	16/06/23 14:10
S-RG10	6773778	601401	1749	spring at RG-A1 front	19/06/22 12:43	NV	16/06/23 14:00
S-RG11	6773867	601367	1738	spring at RG-A1 front	19/06/22 12:35	NV	16/06/23 13:30
S-RG12	6773971	601281	1726	spring at RG-A1 front	NV	18/08/22 11:56 19/08/22 12:10	NV
S-RG13	6773995	601265	1726	spring at RG-A1 front	NV	16/08/22 13:47 18/08/22 11:40	NV

S-RG14	6774166	601183	1712	spring at RG-A1 front	15/06/22 15:30	19/08/22 12:30	NV
					19/06/22 14:25		
S-RG15	6774210	600985	1683	spring at RG-A1 front	19/06/22 15:17	NV	NV
S-RG16	6774034	600854	1740	spring at RG-A1 front	19/06/22 15:42	NV	NV

Table A1: List and description of sites sampled during the three campaigns between June 2022 and August 2023, with UTM coordinates, elevation, dates and times of sampling. Samples are categorized into four distinct types: glacial outlets from the G-B1 glacier snout (S-GL#), ice-debris complex streams in the proglacial area between the glacier tongue and rock glaciers (S-IDC#), Shár Shaw Tagà River (S-R#), and springs from RG-A1 rock glacier front and opposite talus (S-RG#). Sites were not all sampled for every campaign, due to diverse reasons (access and safety issues, no flow, campaign dedicated to a specific area, etc.). When possible, sites were sampled several times to trace potential fluctuations in their physico-chemical signature. When not sampled, the comment "NV" stands for "not visited." The comment "NF," for "no flow," indicates a site not sampled as it was dry when visited.

# Code/Data availability

The data supporting this study are available upon request to the corresponding author.

# Video supplement

576

577

578

579

580

581 582

583584

585

586 587

590591

594

597 598

599

600

- The videos and flight data used for the TIR analysis are available as Supplemental Material in Charonnat and Baraer, 2025, on
- Borealis dataverse (https://doi.org/10.5683/SP3/O57OMY).

#### **Author contribution**

- 592 Conceptualization: B.C. and M.B. Data curation: B.C. Formal analysis: B.C., M.B., J.M.-D. and C.M. Funding acquisition:
- 593 M.B. and J.M.M. Investigation: B.C., M.B., E.V., J.M.-D., K.W. and E.D. Methodology: B.C., M.B., E.V. and J.M.-D. Project
  - administration: B.C., M.B., E.V. and J.M.-D. Supervision: M.B., J.M.-D. and J.M.M. Visualization: B.C. and K.W. Writing –
- original draft preparation: B.C. Writing review & editing: B.C., M.B., E.V., J.M.-D., C.M., K.W., E.D. and J.M.M. All
- authors have read and agreed to the published version of the manuscript.

# Competing interests

The authors declare that they have no conflict of interest.

# Acknowledgements

- We are grateful to the Kluane First Nation and the White River First Nation for the opportunity to conduct research on their
- territory. We thank the Arctic Institute of North America and the University of Calgary for providing us service and access to

- their facilities at Kluane Lake Research Station. We thank Parks Canada for their collaboration and for issuing permits that
- allowed us to conduct research within Kluane National Park and Reserve.

605 606

611

#### Financial support

- This research was supported by the Natural Sciences and Engineering Research Council of Canada, grant numbers RGPIN-
- 608 2020-05612 and RGPNS-2020-05612, and by Natural Resources Canada—Polar Continental Shelf Program, grant number
- 609 62723. Additional funding for the expedition was provided by the Research Centre on the Dynamics of the Earth System
- 610 (GEOTOP).

# References

- 612 Abolt, C., Caldwell, T., Wolaver, B., and Pai, H.: Unmanned aerial vehicle-based monitoring of groundwater inputs to surface
- waters using an economical thermal infrared camera, Optical Engineering, 57(05), 1, https://doi.org/10.1117/1.oe.57.5.053113,
- 614 2018.
- 615 Antonelli, M., Klaus, J., Smettem, K., Teuling, A. J., and Pfister, L.: Exploring Streamwater Mixing Dynamics via Handheld
- Thermal Infrared Imagery, Water, 9(5), Article 5, https://doi.org/10.3390/w9050358, 2017.
- 617 Arenson, L. U., Harrington, J. S., Koenig, C. E. M., and Wainstein, P. A.: Mountain Permafrost Hydrology—A Practical
- Review Following Studies from the Andes, Geosciences, 12(2), Article 2, https://doi.org/10.3390/geosciences12020048, 2022.
- Arenson, L., Hoelzle, M., and Springman, S.: Borehole Deformation Measurements and Internal Structure of Some Rock
- Glaciers in Switzerland, Permafrost and Periglacial Processes, 13, 117–135, https://doi.org/10.1002/ppp.414, 2002.
- 621 Baker, E. A., Lautz, L. K., Kelleher, C. A., and McKenzie, J. M.: The importance of incorporating diurnally fluctuating stream
- 622 discharge in stream temperature energy balance models, Hydrological Processes, 32(18), 2901–2914,
- 623 https://doi.org/10.1002/hyp.13226, 2018.
- 624 Baraer, M., McKenzie, J., Bury, J., and Knox, S.: Characterizing contributions of glacier melt and groundwater during the dry
- 625 season in a poorly gauged catchment of the Cordillera Blanca (Peru), Advances in Geosciences, 22, 41-49,
- 626 https://doi.org/10.5194/adgeo-22-41-2009, 2009.
- 627 Baraer, M., McKenzie, J., Mark, B. G., Gordon, R., Bury, J., Condom, T., Gomez, J., Knox, S., and Fortner, S. K.: Contribution
- of groundwater to the outflow from ungauged glacierized catchments: A multi-site study in the tropical Cordillera Blanca,
- 629 Peru, Hydrological Processes, 29(11), Article 11, https://doi.org/10.1002/hyp.10386, 2015.
- Barclay, J. R., Briggs, M. A., Moore, E. M., Starn, J. J., Hanson, A. E. H., and Helton, A. M.: Where groundwater seeps:
- 631 Evaluating modeled groundwater discharge patterns with thermal infrared surveys at the river-network scale, Advances in
- 632 Water Resources, 160, 104108, https://doi.org/10.1016/j.advwatres.2021.104108, 2022.
- Barsch, D.: Rockglaciers: Indicators for the present and former geoecology in high mountain environments, 1996.

- 634 Bearzot, F., Colombo, N., Cremonese, E., di Cella, U. M., Drigo, E., Caschetto, M., Basiricò, S., Crosta, G. B., Frattini, P.,
- 635 Freppaz, M., Pogliotti, P., Salerno, F., Brunier, A., and Rossini, M.: Hydrological, thermal and chemical influence of an intact
- 636 rock glacier discharge on mountain stream water, Science of The Total Environment, 876, 162777,
- 637 https://doi.org/10.1016/j.scitotenv.2023.162777, 2023.
- 638 Blöthe, J. H., Rosenwinkel, S., Höser, T., and Korup, O.: Rock-glacier dams in High Asia, Earth Surface Processes and
- 639 Landforms, 44(3), 808–824, https://doi.org/10.1002/esp.4532, 2019.
- 640 Bodin, X., Schoeneich, P., Deline, P., Ravanel, L., Magnin, F., Krysiecki, J.-M., and Echelard, T.: Le permafrost de montagne
- et les processus géomorphologiques associés: Évolutions récentes dans les Alpes françaises, Journal of Alpine Research
- Revue de géographie alpine, 103–2, https://doi.org/10.4000/rga.2806, 2015.
- Bolch, T., and Marchenko, S.: Significance of glaciers, rockglaciers and ice-rich permafrost in the Northern Tien Shan as water
- towers under climate change conditions, IHP/HWRP-Berichte, 8, Article 8, <a href="https://doi.org/10.5167/uzh-137250">https://doi.org/10.5167/uzh-137250</a>, 2009.
- Briggs, M. A., Hare, D. K., Boutt, D. F., Davenport, G., and Lane, J. W.: Thermal infrared video details multiscale groundwater
- discharge to surface water through macropores and peat pipes, Hydrological Processes, 30(14), 2510–2511,
- 647 https://doi.org/10.1002/hyp.10722, 2016.
- Brighenti, S., Engel, M., Dinale, R., Tirler, W., Voto, G., and Comiti, F.: Isotopic and chemical signatures of high mountain
- 649 rivers in catchments with contrasting glacier and rock glacier cover, Journal of Hydrology, 623.
- 650 https://doi.org/10.1016/j.jhydrol.2023.129779, 2023.
- 651 Brighenti, S., Tolotti, M., Bruno, M. C., Engel, M., Wharton, G., Cerasino, L., Mair, V., and Bertoldi, W.: After the peak
- water: The increasing influence of rock glaciers on alpine river systems, Hydrological Processes, 33(21), 2804–2823,
- 653 <a href="https://doi.org/10.1002/hyp.13533">https://doi.org/10.1002/hyp.13533</a>, 2019.
- 654 Brunner, P., Therrien, R., Renard, P., Simmons, C. T., and Franssen, H.-J. H.: Advances in understanding river-groundwater
- 655 interactions, Reviews of Geophysics, 55(3), 818–854, https://doi.org/10.1002/2017RG000556, 2017.
- 656 Carrivick, J. L., and Heckmann, T.: Short-term geomorphological evolution of proglacial systems, Geomorphology, 287, 3–
- 28, https://doi.org/10.1016/j.geomorph.2017.01.037, 2017.
- 658 Carturan, L., Zuecco, G., Andreotti, A., Boaga, J., Morino, C., Pavoni, M., Seppi, R., Tolotti, M., Zanoner, T., and Zumiani,
- 659 M.: Spring-water temperature suggests widespread occurrence of Alpine permafrost in pseudo-relict rock glaciers, EGUsphere,
- 1–35, https://doi.org/10.5194/egusphere-2023-2689, 2024.
- 661 Cartwright, I., and Hofmann, H.: Using radon to understand parafluvial flows and the changing locations of groundwater
- 662 inflows in the Avon River, southeast Australia, Hydrology and Earth System Sciences, 20(9), 3581–3600,
- 663 <u>https://doi.org/10.5194/hess-20-3581-2016</u>, 2016.
- 664 Casas-Mulet, R., Pander, J., Ryu, D., Stewardson, M. J., and Geist, J.: Unmanned Aerial Vehicle (UAV)-Based Thermal Infra-
- Red (TIR) and Optical Imagery Reveals Multi-Spatial Scale Controls of Cold-Water Areas Over a Groundwater-Dominated
- Riverscape, Frontiers in Environmental Science, 8, https://doi.org/10.3389/fenvs.2020.00064, 2020.

- 667 Chakravarti, P., Jain, V., and Mishra, V.: The distribution and hydrological significance of intact rock glaciers in the north-
- 668 west Himalaya, Geografiska Annaler, Series A: Physical Geography, 104(3), 226-244,
- https://doi.org/10.1080/04353676.2022.2120262, 2022.
- 670 Charonnat, B. and Baraer, M.: Supplemental Material: Drone-Based Thermal Infrared Imagery for Detection of Cold
- 671 Groundwater Exfiltration in Shár Shaw Tagà, Yukon, Canada, Borealis, V1, https://doi.org/10.5683/SP3/O57OMY, 2025.
- 672 Chesnokova, A., Baraer, M., and Bouchard, É.: Proglacial icings as records of winter hydrological processes, The Cryosphere,
- 673 14(11), 4145–4164, https://doi.org/10.5194/tc-14-4145-2020, 2020.
- 674 Colombo, N., Ferronato, C., Vittori Antisari, L., Marziali, L., Salerno, F., Fratianni, S., D'Amico, M. E., Ribolini, A., Godone,
- D., Sartini, S., Paro, L., Morra di Cella, U., and Freppaz, M.: A rock-glacier pond system (NW Italian Alps): Soil and
- sediment properties, geochemistry, and trace-metal bioavailability, Catena, 194, https://doi.org/10.1016/j.catena.2020.104700,
- 677 2020.
- 678 Colombo, N., Gruber, S., Martin, M., Malandrino, M., Magnani, A., Godone, D., Freppaz, M., Fratianni, S., and Salerno, F.:
- Rainfall as primary driver of discharge and solute export from rock glaciers: The Col d'Olen Rock Glacier in the NW Italian
- 680 Alps, Science of the Total Environment, 639, 316–330, https://doi.org/10.1016/j.scitotenv.2018.05.098, 2018.
- 681 Colombo, N., Salerno, F., Martin, M., Malandrino, M., Giardino, M., Serra, E., Godone, D., Said-Pullicino, D., Fratianni, S.,
- Paro, L., Tartari, G., and Freppaz, M.: Influence of permafrost, rock and ice glaciers on chemistry of high-elevation ponds
- 683 (NW Italian Alps), Science of the Total Environment, 685, 886–901, https://doi.org/10.1016/j.scitotenv.2019.06.233, 2019.
- 684 Colucci, R. R., Forte, E., Žebre, M., Maset, E., Zanettini, C., and Guglielmin, M. Is that a relict rock glacier? Geomorphology,
- 330, 177–189, https://doi.org/10.1016/j.geomorph.2019.02.002, 2019.
- 686 Croce, F., and Milana, J.: Internal structure and behavior of a Rock Glacier in the arid Andes of Argentina, Permafrost and
- 687 Periglacial Processes, 13, 289–299, https://doi.org/10.1002/ppp.431, 2002.
- 688 Delaloye, R., Lambiel, C., and Gärtner-Roer, I.: Overview of rock glacier kinematics research in the Swiss Alps: Seasonal
- 689 rhythm, interannual variations and trends over several decades, Geographica Helvetica, 65(2), 135–145,
- 690 https://doi.org/10.5194/gh-65-135-2010, 2010.
- 691 Dodds, C.J., and Campbell, R.B.: Overview, legend and mineral deposit tabulations for: GSC Open File 2188 to Open File
- 692 2191, Geological Survey of Canada, Energy Mines and Resources Canada, 85 p. + 5 maps, 1992.
- 693 Dugdale S. J.: A practitioner's guide to thermal infrared remote sensing of rivers and streams: recent advances, precautions
- and considerations, WIREs Water, vol. 3, no. 2, pp. 251–268, https://doi.org/10.1002/wat2.1135, 2016.
- 695 Engel, M., Penna, D., Bertoldi, G., Vignoli, G., Tirler, W., and Comiti, F.: Controls on spatial and temporal variability in
- streamflow and hydrochemistry in a glacierized catchment, Hydrology and Earth System Sciences, 23(4), 2041-2063,
- 697 https://doi.org/10.5194/hess-23-2041-2019, 2019.
- Ensom, T., Makarieva, O., Morse, P., Kane, D., Alekseev, V., and Marsh, P.: The distribution and dynamics of aufeis in
- permafrost regions, Permafrost and Periglacial Processes, 31(3), 383–395, https://doi.org/10.1002/ppp.2051, 2020.

- Evin, M., Fabre, D., and Johnson, P. G.: Electrical Resistivity Measurements on the Rock Glaciers of Grizzly Creek, St Elias
- Mountains, Yukon, Permafrost and Periglacial Processes, 8, 11, 1997.
- Falatkova, K., Šobr, M., Slavík, M., Bruthans, J., and Janský, B.: Hydrological characterization and connectivity of proglacial
- lakes to a stream, Adygine ice-debris complex, northern Tien Shan, Hydrological Sciences Journal, 65(4), 610-623,
- 704 https://doi.org/10.1080/02626667.2020.1711913, 2020.
- 705 Frauenfelder, R., Allgöwer, B., Haeberli, W., and Hoelzle, M.: Permafrost investigations with GIS a case study in the
- 706 Fletschhorn area, Wallis, Swiss Alps, In Permafrost, Proceedings of the Seventh International Conference, 23–27 June 1998,
- 707 Yellowknife, Canada, Lewkowicz AG, Allard M (eds) eds, Collection Nordicana 57, Centre d'études Nordiques, Université
- 708 Laval: Québec; 291–295, 1998.
- 709 Gibson J.J., Holmes T., Stadnyk T.A., Birks S.J., Eby P., and Pietroniro A.: 18O and 2H in streamflow across Canada, Journal
- 710 of Hydrology: Regional Studies, Volume 32, 100754, ISSN 2214-5818, <a href="https://doi.org/10.1016/j.ejrh.2020.100754">https://doi.org/10.1016/j.ejrh.2020.100754</a>, 2020.
- 711 Haeberli, W.: Untersuchungen zur Verbreitung von Permafrost zwischen Flüelapass und Piz Grialetsch (Graubünden),
- 712 Mitteilungen der VAW ETH Zürich 17: 1–221, 1975.
- Halla, C., Henrik Blöthe, J., Tapia Baldis, C., Trombotto Liaudat, D., Hilbich, C., Hauck, C., and Schrott, L.: Ice content and
- 714 interannual water storage changes of an active rock glacier in the dry Andes of Argentina, Cryosphere, 15(2), 1187–1213,
- 715 https://doi.org/10.5194/tc-15-1187-2021, 2021.
- 716 Harrington, J. S., Mozil, A., Hayashi, M., and Bentley, L. R.: Groundwater flow and storage processes in an inactive rock
- 717 glacier, Hydrological Processes, 32(20), 3070–3088, https://doi.org/10.1002/hyp.13248, 2018.
- 718 Harrison, S., Jones, D., Anderson, K., Shannon, S., and Betts, R. A.: Is ice in the Himalayas more resilient to climate change
- 719 than we thought? Geografiska Annaler, Series A: Physical Geography, 103(1), 1-7,
- 720 https://doi.org/10.1080/04353676.2021.1888202.2021.
- 721 Hayashi, M.: Alpine Hydrogeology: The Critical Role of Groundwater in Sourcing the Headwaters of the World. Groundwater,
- 722 58(4), 498–510, https://doi.org/10.1111/gwat.12965, 2020.
- 723 Hem, J. D.: Study and Interpretation of the Chemical Characteristics of Natural Water, 3rd Edition, US Geological Survey
- Water-Supply Paper 2254, University of Virginia, Charlottesville, 263 p., https://doi.org/10.3133/wsp2254, 1985.
- 725 Hewitt, K.: Rock Glaciers and Related Phenomena. In K. Hewitt (Ed.), Glaciers of the Karakoram Himalaya: Glacial
- Environments, Processes, Hazards and Resources (pp. 267–289), Springer Netherlands, https://doi.org/10.1007/978-94-007-
- 727 6311-1 11, 2014.
- Hock, R., Rasul, G., Adler, C., Cáceres, B., Gruber, S., Hirabayashi, Y., Jackson, M., Kääb, A., Kang, S., Kutuzov, S., Milner,
- Al., Molau, U., Morin, S., Orlove, B., and Steltzer, H.: High Mountain Areas. In: IPCC Special Report on the Ocean and
- 730 Cryosphere in a Changing Climate [Pörtner, H.-O., Roberts, D.C., Masson-Delmotte, V., Zhai, P., Tignor, M., Poloczanska,
- E., Mintenbeck, K., Alegría, A., Nicolai, M., Okem, A., Petzold, J., Rama, B. and Weyer N.M. (eds.)]: Cambridge University
- 732 Press, Cambridge, UK and New York, NY, USA, pp. 131-202, https://doi.org/10.1017/9781009157964.004, 2019.

- Huss, M., Bookhagen, B., Huggel, C., Jacobsen, D., Bradley, R. S., Clague, J. J., Vuille, M., Buytaert, W., Cayan, D. r.,
- 734 Greenwood, G., Mark, B. g., Milner, A. M., Weingartner, R., and Winder, M.: Toward mountains without permanent snow
- 735 and ice, Earth's Future, 5(5), 418–435, https://doi.org/10.1002/2016EF000514, 2017.
- 736 Iwasaki, K., Fukushima, K., Nagasaka, Y., Ishiyama, N., Sakai, M., and Nagasaka, A.: Real-Time Monitoring and
- 737 Postprocessing of Thermal Infrared Video Images for Sampling and Mapping Groundwater Discharge, Water Resources
- 738 Research, 59(4), e2022WR033630, https://doi.org/10.1029/2022WR033630, 2023.
- 739 Iwasaki, K., Nagasaka Y., Ishiyama N., and Nagasaka A.: Thermal imaging survey for characterizing bedrock groundwater
- 740 discharge: comparison between sedimentary and volcanic catchments, Hydrological Research Letters 18(3): 79-86,
- 741 http://dx.doi.org/10.3178/hrl.18.79, 2024.
- Johnson, P. G.: Rock glacier types and their drainage systems, Grizzly Creek, Yukon Territory, Canadian Journal of Earth
- 743 Sciences, 15(9), 1496–1507, https://doi.org/10.1139/e78-155, 1978.
- Jones, D. B., Harrison, S., Anderson, K., and Betts, R. A.: Mountain rock glaciers contain globally significant water stores,
- 745 Scientific Reports, 8(1), Article 1, https://doi.org/10.1038/s41598-018-21244-w, 2018.
- Jones, D. B., Harrison, S., Anderson, K., Shannon, S., and Betts, R. A.: Rock glaciers represent hidden water stores in the
- 747 Himalaya, Science of The Total Environment, 793, 145368, https://doi.org/10.1016/j.scitotenv.2021.145368, 2021.
- Jones, D. B., Harrison, S., Anderson, K., and Whalley, W. B.: Rock glaciers and mountain hydrology: A review, Earth-Science
- 749 Reviews, 193, 66–90, https://doi.org/10.1016/j.earscirev.2019.04.001, 2019.
- 750 Kalbus, E., Reinstorf, F., and Schirmer, M.: Measuring methods for groundwater and surface water interactions: review,
- 751 Hydrology and Earth System Sciences, 10(6), 873–887, https://doi.org/10.5194/hess-10-873-2006, 2006.
- 752 Käser, D., and Hunkeler, D.: Contribution of alluvial groundwater to the outflow of mountainous catchments, Water Resources
- 753 Research, 52(2), 680–697, https://doi.org/10.1002/2014WR016730, 2016.
- 754 Krainer, K., and Mostler, W.: Hydrology of Active Rock Glaciers: Examples from the Austrian Alps, Arctic, Antarctic, and
- 755 Alpine Research, 34(2), 142–149, https://doi.org/10.1080/15230430.2002.12003478, 2002.
- 756 Krainer, K., Mostler, W., and Spötl, C.: Discharge from active rock glaciers, Austrian Alps: A stable isotope approach, Austrian
- 757 Journal of Earth Sciences, 100, 102–112, 2007.
- 758 Kummert, M., Bodin, X., Braillard, L., and Delaloye, R.: Pluri-decadal evolution of rock glaciers surface velocity and its
- 759 impact on sediment export rates towards high alpine torrents, Earth Surface Processes and Landforms, 46(15), 3213–3227,
- 760 <u>https://doi.org/10.1002/esp.5231</u>, 2021.
- 761 Lloyd, S.: Least squares quantization in PCM, IEEE Transactions on Information Theory, 28(2), 129–137, IEEE Transactions
- on Information Theory, <a href="https://doi.org/10.1109/TIT.1982.1056489">https://doi.org/10.1109/TIT.1982.1056489</a>, 1982.
- 763 MacQueen, J.: Some methods for classification and analysis of multivariate observations, In Proceedings of the fifth Berkeley
- symposium on mathematical statistics and probability (Vol. 1, No. 14, pp. 281-297), 1967.

- Marcer, M., Cicoira, A., Cusicanqui, D., Bodin, X., Echelard, T., Obregon, R., and Schoeneich, P.: Rock glaciers throughout
- 766 the French Alps accelerated and destabilised since 1990 as air temperatures increased, Communications Earth & Environment,
- 767 2(1), 1–11, https://doi.org/10.1038/s43247-021-00150-6, 2021.
- Marren, P. M., and Toomath, S. C.: Channel pattern of proglacial rivers: Topographic forcing due to glacier retreat, Earth
- 769 Surface Processes and Landforms, 39(7), 943–951, https://doi.org/10.1002/esp.3545, 2014.
- 770 Müller, T., Roncoroni, M., Mancini, D., Lane, S. N., and Schaefli, B.: Current and future roles of meltwater-groundwater
- 771 dynamics in a proglacial Alpine outwash plain, Hydrology and Earth System Sciences, 28(4), 735–759,
- 772 https://doi.org/10.5194/hess-28-735-2024, 2024.
- Navarro, G., Valois, R., MacDonell, S., de Pasquale, G., and Díaz, J. P.: Internal structure and water routing of an ice-debris
- 1774 landform assemblage using multiple geophysical methods in the semiarid Andes, Frontiers in Earth Science, 11,
- 775 https://doi.org/10.3389/feart.2023.1102620, 2023.
- PERMOS Report 2019-16-19 | PERMOS Swiss Permafrost Monitorinig Network, Retrieved 17 September 2024, from
- https://www.permos.ch/doi/permos-rep-2019-16-19, 2019.
- Porter, C., Howat, I., Noh, M.-J., Husby, E., Khuvis, S., Danish, E., Tomko, K., Gardiner, J., Negrete, A., Yadav, B., Klassen,
- J., Kelleher, C., Cloutier, M., Bakker, J., Enos, J., Arnold, G., Bauer, G., and Morin, P.: ArcticDEM Mosaics, Version 4.1
- 780 [Dataset], Harvard Dataverse, https://doi.org/10.7910/DVN/3VDC4W, 2023.
- 781 Rautio, A., Kivimäki, A.-L., Korkka-Niemi, K., Nygård, M., Salonen, V.-P., Lahti, K., and Vahtera, H.: Vulnerability of
- 782 groundwater resources to interaction with river water in a boreal catchment, Hydrology and Earth System Sciences, 19(7),
- 783 3015–3032, https://doi.org/10.5194/hess-19-3015-2015, 2015.
- Reato, A., Borzi, G., Martínez, O. A., and Carol, E.: Role of rock glaciers and other high-altitude depositional units in the
- 785 hydrology of the mountain watersheds of the Northern Patagonian Andes, Science of The Total Environment, 824, 153968.
- 786 https://doi.org/10.1016/j.scitotenv.2022.153968, 2022.
- 787 Scapozza, C.: Contributo dei metodi termici alla prospezione del permafrost montano: esempi dal massiccio della Cima di
- 788 Gana Bianca (Val Blenio, Svizzera), Bollettino della Società Ticinese di Scienze Naturali 97:55–66, 2009.
- 789 Scapozza, C.: Investigation on protalus ramparts in the Swiss Alps, Geographica Helvetica, 70(2), 135–139,
- 790 https://doi.org/10.5194/gh-70-135-2015, 2015.
- 791 Schreder, S., Sommaruga, R., Psenner, R., Chimani, B., Ganekind, M., and Koinig, K. A.: Changes in air temperature, but not
- 792 in precipitation, determine long-term trends in water chemistry of high mountain lakes of the Alps with and without rock
- 793 glacier influence, Science of the Total Environment, 905, https://doi.org/10.1016/j.scitotenv.2023.167750, 2023.
- 794 Scotti, R., Crosta, G. B., and Villa, A.: Destabilisation of Creeping Permafrost: The Plator Rock Glacier Case Study (Central
- 795 Italian Alps), Permafrost and Periglacial Processes, 28(1), 224–236, https://doi.org/10.1002/ppp.1917, 2017.
- 796 Sorg, A., Kääb, A., Roesch, A., Bigler, C., and Stoffel, M.: Contrasting responses of Central Asian rock glaciers to global
- warming, Scientific Reports, 5, https://doi.org/10.1038/srep08228, 2015.

- 798 Toran, L.: Groundwater-Surface Water Interaction, In Encyclopedia of Water (pp. 1-12), John Wiley & Sons, Ltd,
- 799 https://doi.org/10.1002/9781119300762.wsts0027, 2019.
- 800 Torgersen C. E., Faux R. N., McIntosh B. A., Poage N. J., and Norton D. J.: Airborne thermal remote sensing for water
- temperature assessment in rivers and streams, Remote Sensing of Environment, vol. 76, no. 3, pp. 386-398,
- 802 https://doi.org/10.1016/S0034-4257(01)00186-9, 2001.
- 803 Tronstad, L. M., Hotaling, S., Giersch, J. J., Wilmot, O. J., and Finn, D. S.: Headwaters Fed by Subterranean Ice: Potential
- 804 Climate Refugia for Mountain Stream Communities? Western North American Naturalist, 80(3), 395-407,
- 805 https://doi.org/10.3398/064.080.0311, 2020.
- van Tiel, M., Aubry-Wake, C., Somers, L., Andermann, C., Avanzi, F., Baraer, M., Chiogna, G., Daigre, C., Das, S., Drenkhan,
- 807 F., Farinotti, D., Fyffe, C. L., de Graaf, I., Hanus, S., Immerzeel, W., Koch, F., McKenzie, J. M., Müller, T., Popp, A. L., ...
- Yapiyev, V.: Cryosphere–groundwater connectivity is a missing link in the mountain water cycle, Nature Water, 2(7), 624–
- 809 637, https://doi.org/10.1038/s44221-024-00277-8, 2024.
- Vélez-Nicolás, M., García-López, S., Barbero, L., Ruiz-Ortiz, V., and Sánchez-Bellón, Á.: Applications of Unmanned Aerial
- Systems (UASs) in Hydrology: A Review, Remote Sensing, 13(7), Article 7, https://doi.org/10.3390/rs13071359, 2021.
- Wagner, T., Brodacz, A., Krainer, K., and Winkler, G.: Active rock glaciers as shallow groundwater reservoirs, Austrian Alps,
- 813 Grundwasser, 25(3), 215–230, https://doi.org/10.1007/s00767-020-00455-x, 2020.
- 814 Wagner, T., Kainz, S., Krainer, K., and Winkler, G.: Storage-discharge characteristics of an active rock glacier catchment in
- the Innere Ölgrube, Austrian Alps, Hydrological Processes, 35(5), https://doi.org/10.1002/hyp.14210, 2021.
- Wagner, T., Pauritsch, M., and Winkler, G.: Impact of relict rock glaciers on spring and stream flow of alpine watersheds:
- 817 Examples of the Niedere Tauern Range, Eastern Alps (Austria), Austrian Journal of Earth Sciences, 109(1),
- 818 https://doi.org/10.17738/ajes.2016.0006, 2016.
- Wahl, H. E., Fraser, D. B., Harvey, R. C., and Maxwell, J. B.: Climate of Yukon, Atmospheric Environment Service,
- 820 Environment Canada, 1987.
- Wanner, C., Moradi, H., Ingold, P., Cardenas Bocanegra, M. A., Mercurio, R., and Furrer, G.: Rock glaciers in the Central
- 822 Eastern Alps How permafrost degradation can cause acid rock drainage, mobilization of toxic elements and formation of
- basaluminite, Global and Planetary Change, 227, https://doi.org/10.1016/j.gloplacha.2023.104180, 2023.
- Webb, B. W., Hannah, D. M., Moore, R. D., Brown, L. E., and Nobilis, F.: Recent advances in stream and river temperature
- 825 research, Hydrological Processes, 22(7), 902–918, https://doi.org/10.1002/hyp.6994, 2008.
- Winkler, G., Wagner, T., Pauritsch, M., and Kellerer-Pirklbauer, A.: What will occur after permafrost? Relevance of relict
- rock glaciers for the discharge behaviour of alpine catchments, Joannea Geologie und Palaontologie, 12, 63–72, 2016.
- 828 Zappa C. J., Jessup A. T., and Yeh H.: Skin layer recovery of free-surface wakes: Relationship to surface renewal and
- dependence on heat flux and background turbulence, Journal of Geophysical Research: Oceans, vol. 103, no. C10, pp. 21711–
- 830 21722, 1998, https://doi.org/10.1029/98JC01942, 1998.

- 831 Zarroca, M., Roqué, C., Linares, R., Salminci, J. G., and Gutiérrez, F.: Natural acid rock drainage in alpine catchments: A side
- effect of climate warming, Science of The Total Environment, 778, 146070, https://doi.org/10.1016/j.scitotenv.2021.146070,
- 833 2021.
- 834 Zierl, B., and Bugmann, H.: Global change impacts on hydrological processes in Alpine catchments, Water Resources
- 835 Research, 41(2), <a href="https://doi.org/10.1029/2004WR003447">https://doi.org/10.1029/2004WR003447</a>, 2005.